AGU PUBLICATIONS

Global Biogeochemical Cycles

RESEARCH ARTICLE

10.1002/2017GB005736

Key Points:
- Surface dissolved iron concentrations are elevated near continental Australia and decreased eastward in the South Pacific gyre
- Model calculations suggest that a significant portion of dissolved iron within the remote surface ocean is sourced from the atmosphere
- The supply stoichiometry for iron and nitrogen relative to phosphate declines eastward leading to two biogeographical provinces

Supporting Information:
- Supporting Information S1

Correspondence to:
M. J. Ellwood,
michael.ellwood@anu.edu.au

Citation:
Ellwood, M. J., Bowie, A. R., Baker, A., Gault-Ringold, M., Hassler, C., Law, C. S., … Boyd, P. W. (2018). Insights into the biogeochemical cycling of iron, nitrate, and phosphate across a 5,300 km South Pacific zonal section (153°E–150°W). *Global Biogeochemical Cycles*, *32*. https://doi.org/10.1002/2017GB005736

Received 2 JUN 2017
Accepted 22 DEC 2017
Accepted article online 4 JAN 2018

Insights Into the Biogeochemical Cycling of Iron, Nitrate, and Phosphate Across a 5,300 km South Pacific Zonal Section (153°E–150°W)

Michael J. Ellwood[1], Andrew R. Bowie[2,3], Alex Baker[4], Melanie Gault-Ringold[2,5], Christel Hassler[6], Cliff S. Law[5,7], William A. Maher[8], Andrew Marriner[7], Scott Nodder[7], Sylvia Sander[5], Craig Stevens[7,9], Ashley Townsend[10], Pier van der Merwe[2], E. Malcolm S. Woodward[11], Kathrin Wuttig[2], and Philip W. Boyd[5,7,12]

[1]Research School of Earth Sciences, Australian National University, Canberra, ACT, Australia, [2]Antarctic Climate and Ecosystems Cooperative Research Centre, Hobart, Tasmania, Australia, [3]Institute for Marine and Antarctic Studies, University of Tasmania, Hobart, Tasmania, Australia, [4]Centre for Ocean and Atmospheric Sciences, School of Environmental Sciences, University of East Anglia, Norwich, UK, [5]Department of Chemistry, University of Otago, Dunedin, New Zealand, [6]Department F.-A. Forel for Environmental and Aquatic Sciences, University of Geneva, Geneva, Switzerland, [7]National Institute of Water and Atmospheric Research, Wellington, New Zealand, [8]Institute for Applied Ecology, University of Canberra, Canberra, ACT, Australia, [9]Department of Physics, University of Auckland, Auckland, New Zealand, [10]Central Science Laboratory, University of Tasmania, Hobart, Tasmania, Australia, [11]Plymouth Marine Laboratory, Plymouth, UK, [12]Now at Institute for Marine and Antarctic Studies, University of Tasmania, Hobart, Tasmania, Australia

Abstract Iron, phosphate, and nitrate are essential nutrients for phytoplankton growth, and hence, their supply into the surface ocean controls oceanic primary production. Here we present a GEOTRACES zonal section (GP13; 30–33°S, 153°E–150°W) extending eastward from Australia to the oligotrophic South Pacific Ocean gyre outlining the concentrations of these key nutrients. Surface dissolved iron concentrations are elevated at >0.4 nmol L^{-1} near continental Australia (west of 165°E) and decreased eastward to ≤ 0.2 nmol L^{-1} (170°W–150°W). The supply of dissolved iron into the upper ocean (<100 m) from the atmosphere and vertical diffusivity averaged 11 ± 10 nmol m^{-2} d^{-1}. In the remote South Pacific Ocean (170°W–150°W), atmospherically sourced iron is a significant contributor to the surface dissolved iron pool with average supply contribution of 23 ± 17% (range 3% to 55%). Surface water nitrate concentrations averaged 5 ± 4 nmol L^{-1} between 170°W and 150°W, while surface water phosphate concentrations averaged 58 ± 30 nmol L^{-1}. The supply of nitrogen into the upper ocean is primarily from deeper waters (24–1647 μmol m^{-2} d^{-1}) with atmospheric deposition and nitrogen fixation contributing <1% to the overall flux along the eastern part of the transect. The deep water N:P ratio averaged 14.5 ± 0.5 but declined to <1 above the deep chlorophyll maximum (DCM) indicating a high N:P assimilation ratio by phytoplankton leading to almost quantitative removal of nitrate. The supply stoichiometry for iron and nitrogen relative to phosphate at and above the DCM declines eastward leading to two biogeographical provinces: one with diazotroph production and the other without diazotroph production.

Plain Language Summary Iron, phosphate, and nitrate are essential nutrients for phytoplankton growth and hence their supply into the surface ocean controls phytoplankton growth. We present a 5,300 km zonal section extending from Australia into the South Pacific Ocean relating to iron, nitrate, and phosphate. We find that the supply of these nutrients into the surface ocean defines that biogeographical distribution of phytoplankton groups.

1. Introduction

Phytoplankton productivity in open ocean waters is primarily controlled by the availability of the macronutrients nitrogen and phosphorus, and the micronutrient iron (Falkowski et al., 1998; Martin & Fitzwater, 1988; Moore et al., 2013, 2004; Saito et al., 2014). In oligotrophic waters, such as in the South Pacific Gyre (defined here as tropical and subtropical waters) (Figure 1), phytoplankton production can be limited via the low concentrations of nitrogen, phosphorus, and iron within the euphotic zone (Bonnet et al., 2008; Moisander et al., 2012; Saito et al., 2014; Van Wambeke et al., 2008). In this regard, the South Pacific Gyre is regarded as an ultraoligotrophic region because the vertical supply of nitrogen into the euphotic zone is

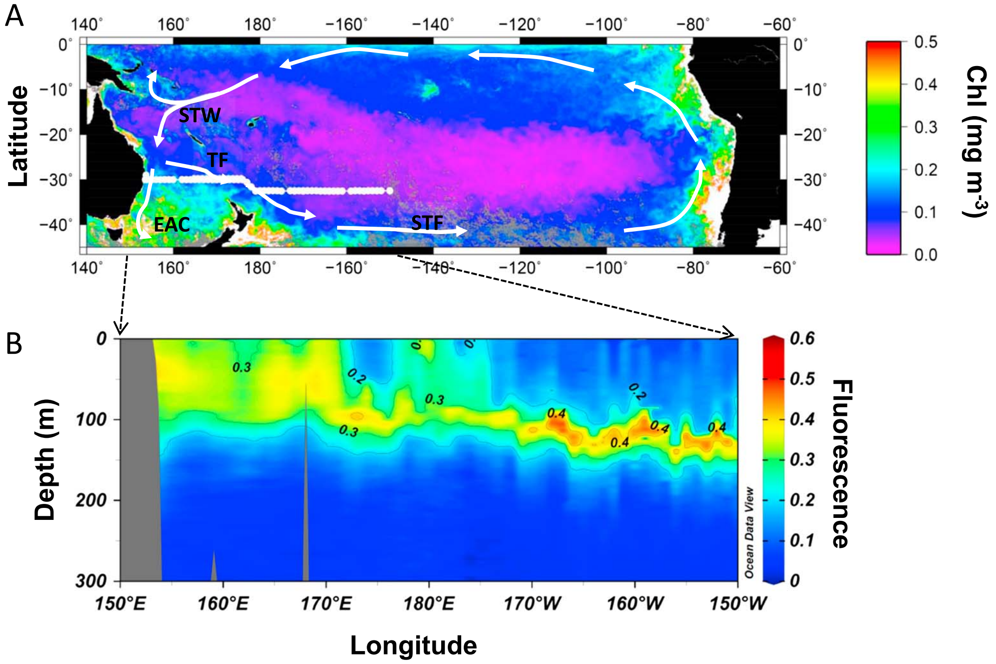

Figure 1. (a) Satellite-derived chlorophyll (Chl) concentrations for the South Pacific Ocean for the period 16 May to 16 June 2011 (1 month composite) inclusive. (b) Water column fluorescence. Figures were generated using Generic Mapping Tools (Wessel & Smith, 1998) and Ocean Data View (Schlitzer, 2006). Satellite data were obtained from ERDDAP (http://coastwatch.pfeg.noaa.gov/erddap/index.html). Note that the CTD fluorescence data from the Australian leg (153°E to 170°W) was rescaled to the fluorescence data obtained on the New Zealand leg (170°W to 150°W). The white arrows in Figure 1a represent the general surface water flow patterns and the general bounds for the South Pacific Gyre (Chiswell et al., 2015; Ridgway & Dunn, 2007). STW = subtropical water, EAC = East Australian Current, STF = subtropical front.

governed by the depth of nitracline and also by low rates of nitrogen fixation within surface waters (Halm et al., 2012; Law et al., 2012; Raimbault & Garcia, 2008). Indeed, primary production within the center of the South Pacific Gyre is extremely low (~0.15 g C m^{-2} d^{-1}) and is predominantly driven by the regeneration of nutrients within the surface ocean (Bonnet et al., 2008; Raimbault & Garcia, 2008; Raimbault et al., 2008).

The South Pacific Gyre is bounded by the equator to the north, the land masses of Australia and South America to the west and east respectively, and the Southern Ocean to the south (Figure 1). The general circulation of the gyre is anticyclonic with westward-moving currents along the northern boundary of the gyre near the equator and eastward-moving currents along the southern boundary. Below the surface, the major currents entering the South Pacific basin from the south are Antarctic Bottom Water (AABW), Lower Circumpolar Deep Water (LCDW), Antarctic Intermediate Water (AAIW), and Subantarctic Mode Water (SAMW) (Chiswell et al., 2015; Wijffels et al., 2001). The main southward penetrating water masses in the South Pacific basin is North Pacific Deep Water (NPDW) (Figure S1 in the supporting information).

Dissolved iron concentrations in South Pacific surface waters are generally low with concentrations at or below 0.15 nmol L^{-1} (Blain et al., 2008; Chappell et al., 2012; Ellwood et al., 2013; Fitzsimmons et al., 2014; Hassler et al., 2014). At these low concentrations, both community and diazotroph primary production would appear to be iron-limited (Bonnet et al., 2008; Shiozaki et al., 2014; Ward et al., 2013). Incubation experiments undertaken in central South Pacific waters reported that additions of iron did not stimulate nitrogen fixation (Bonnet et al., 2008; Raimbault & Garcia, 2008), suggesting chronic iron limitation of diazotroph production (i.e., cells unable to upregulate nitrogen fixation) and/or the absence of nitrogen fixers (Law et al., 2011).

Adjacent to continental land masses, such as Australia, surface dissolved iron concentrations tend to be higher than in offshore waters as a result of higher iron inputs associated with dust and coastal upwelling (Cropp et al., 2013; Law et al., 2011, 2012; Shaw et al., 2008; Wagener et al., 2008). Surface dissolved iron concentrations also tend to decrease as the iron supply flux declines downstream from continental dust sources

(Moisander et al., 2012). The supply of atmospheric iron to South Pacific waters is relatively low in global terms (Arimoto et al., 1987, 1990; Buck et al., 2013; Halstead et al., 2000; Wagener et al., 2008), because of its remoteness to potential iron-rich dust sources, however it may play a disproportionately large role in setting upper ocean iron inventories in this region when vertical and lateral diffusivity and mixing are low (Chiswell, 2013; Zhurbas & Oh, 2004).

The depth of the ferricline in the South Pacific Ocean (defined here as the depth at which the change in the concentration of dissolved iron with depth (∂DFe/∂z) is greatest) is deepest away from hydrothermal sources (e.g., Tonga-Kermadec Ridge system close to the international dateline) and is typically $>$200 m deeper than that of the nitracline (Blain et al., 2008). Recent analysis of ferricline depth for the Southern Ocean reveals that it is also much deeper than that of the nitracline ($\partial NO_3/\partial z$) and phosphocline ($\partial PO_4/\partial z$) (Tagliabue et al., 2014). This observation is particularly important as the depth and the magnitude of the dissolved iron concentration gradient across the ferricline sets the magnitude of the dissolved iron flux to the euphotic zone (Blain et al., 2008; Boyd & Ellwood, 2010; de Baar et al., 1995; Johnson et al., 1997; Tagliabue et al., 2014). The depth of this feature can be highly influential in regions such as the South Pacific gyre where dust inputs are low (Buck et al., 2013; Wagener et al., 2008). The decoupling between the depths of the ferricline and nitracline/phosphocline also influences the stoichiometric supply of elements to the resident phytoplankton community, which in turn influences the composition of the phytoplankton community and their relative depth in the water column. For the South Pacific basin, the depth at which the ferricline, nitracline, and phosphocline occur relative to the DCM is not well established.

Recent modeling efforts to unify observation work have focused on defining the role the stoichiometric supply of iron, nitrogen, and phosphate have on the structure and function of phytoplankton communities (Moore et al., 2013; Ward et al., 2013). Modeling by Ward et al. (2013) shows that the observed global biogeography of diazotrophs and non-diazotrophs can be reproduced by manipulation of the stoichiometric supply ratios of iron, nitrate, and phosphate to the surface ocean. They defined six functional biogeochemical provinces for the global ocean. The two regions applicable to the GP13 section across the Southwest Pacific Ocean are the “surplus phosphate, no diazotrophs” (SPND) and “surplus phosphate, with diazotrophs” (SPD). In the Ward et al. (2013) study, the SPND province is defined as being “characterized by the absence of diazotrophs, with low surface dissolved inorganic nitrogen, elevated surface dissolved inorganic phosphate, and slightly elevated (but still low) surface dissolved iron” and the SPD province is defined where the “dissolved inorganic nitrogen and dissolved iron are drawn down to subsistence concentrations by the non-diazotrophs and diazotrophs, respectively, and the supply of excess inorganic phosphate is balanced by local accumulation and dispersal”. Ward et al. (2013) varied N:P and Fe:N stoichiometric supply ratios within a number of model simulations thus allowing them to project the likely N:P and Fe:N stoichiometric conditions under which the SPND and SPD provinces are likely to form. The aim of this GEOTRACES zonal survey stretching from Australia (154°E) to south of Tahiti (150°W) along ~30°S was to assess the distribution of iron and macronutrient concentrations across the Southwest Pacific Ocean; evaluate the depth of the ferricline relative to that of the nitracline, phosphocline, and the DCM; and characterize the relative supply and stoichiometry of iron, nitrogen, and phosphate to the surface ocean from above and below, thereby allowing us to determine likely biogeochemical provinces for the region. We also explore the regenerational supply of iron to thermocline waters zonally to determine the potential influence atmospheric supply has on intermediate water masses. This study forms part of the GEOTRACES effort to map the distribution of trace element concentrations and isotopes within the global ocean (Mawji et al., 2015).

2. Methods

2.1. Voyage Tracks and Water Masses

The western South Pacific ANZ zonal GP13 section was jointly undertaken by Australian and New Zealand voyages from 154°E to 150°W between 30 and 32.5°S (Figure 1). The GP13 zonal transect is a repeat section of a prior World Ocean Circulation Experiment line (P06). The regional aims were to (1) characterize the East Australian Current (EAC) adjacent to Australia as it meanders along the Tasman Front toward New Zealand and also to investigate the return flow of the Southern Hemisphere “supergyre” (Ridgway & Dunn, 2007) as it turns southward along the shelf-break off eastern Australia (GEOTRACES, 2007) and (2) characterize the supply of iron, nitrate, and phosphate into the euphotic zone and their cycling within the gyre. At depth, the

GP13 section provides a narrow cross-section of the nutrient and trace metal concentration profiles of the Deep Western Boundary Current entering the Pacific Basin from the south. A complementary paper focusing on the deep water supply and lateral transport of trace elements along the GP13 section is in preparation.

The first sector of GP13 utilized the R/V *Southern Surveyor* (Australia) and was undertaken in austral autumn (13 May 2011 and 6 June 2011) from 152°E; 30°S to 170°W; 32.5°S. GEOTRACES crossover stations, for intercalibration of the hydrography, trace metal, and nutrient results, were occupied at 170°W (31 May 2011) and 172°W (1 June 2011). The second sector of GP13 utilized the R/V *Tangaroa* (New Zealand). This voyage was undertaken in the austral winter (6 June 2011 to 30 June 2011) and went from 170°W; 32.5°S to 150°W; 32.5°S with reoccupation of crossover stations on 10 and 11 June 2011, respectively. The sampling strategies for the two voyages were to collect dissolved trace metal and nutrient samples from the surface to the seafloor at every 5° of longitude, and surface to 1500 m at every 1° of longitude. Complementary conductivity-temperature-depth (CTD) casts were collected at each station for standard parameters such as pressure, temperature, salinity, and fluorescence along with a limited number of samples for dissolved oxygen used to calibrate CTD values.

2.2. Ship-Based CTD Profiling

Conductivity-temperature-depth (CTD) profile data and water samples for nutrient and biological parameters were collected with a winch-lowered package consisting of an SBE 911plus CTD, a Turner Designs fluorometer, and a 24-bottle SBE 32 Carousel water sampler. The dual temperature (SBE 3plus), conductivity (SBE 4plus), and pressure sensors (Paroscientific) were calibrated at the SBE calibration facility. In situ salinity water samples were measured with a Guildline salinometer, standardized with International Association for the Physical Sciences of the Ocean standard seawater. Some light quenching of the fluorescence signal may have occurred at some stations as fluorescence measurements were not all made at night. This was not expected to have a strong influence on the fluorescence data set as the depth of the DCM was expected to be deep (>50 m) across most of the section. Active fluorescence (F_v/F_m) measurements were also made on a select number of samples collected from the CTD-rosette package.

2.3. Trace Metal Sampling

On both voyages, seawater samples for trace metal determination were collected using acid-cleaned, Teflon-coated, externally sprung, 10 L Niskin bottles attached to an autonomous rosette (Model 1018, General Oceanics, USA). Upon retrieval, the Niskin bottles were transferred into a clean container laboratory fitted with HEPA-filtered air work stations. Seawater samples for dissolved trace metal analysis were filtered through acid-cleaned 0.2-μm capsule filters (Supor AcroPak 200, Pall) and acidified with either distilled nitric acid (New Zealand leg) or hydrochloric acid (Australian leg) to a final pH $\leq$ 1.8. The sampling protocols followed recommendations in the "GEOTRACES Cookbook" (http://www.geotraces.org/science/intercalibration/222-sampling-and-sample-handling-protocols-for-geotraces-cruises).

2.4. Nutrient and Trace Metal Determination

Dissolved nutrient concentrations (nitrate, nitrite, phosphate, and silicate) were determined at sea by automated analysis using a segmented flow colorimetric autoanalyzer with digital detection (Frew et al., 2001; Woodward & Rees, 2001). The micromolar nutrients on the NZ voyage were checked and quality controlled by the regular analysis of suitable concentration nutrient reference materials (KANSO, Japan). On the New Zealand GP13 leg, nanomolar nutrient concentrations of nitrate, nitrite, and phosphate measurements were also made using a three-channel nanomolar analyzer, with segmented flow colorimetric analytical techniques in combination with a 2 m flow length Liquid Waveguide Capillary Cell (Woodward, 2002; Woodward & Rees, 2001). The detection limit for the nanonutrient system used at selected stations on the New Zealand leg of the ANZ section was ~0.5 nmol L^{-1} for nitrate and nitrite, and <1 nmol L^{-1} for phosphate.

For samples collected on the New Zealand leg, iron and supporting trace metals were either determined by isotope dilution using enriched isotopes (^{57}Fe, ^{67}Zn, ^{65}Cu, ^{61}Ni, ^{110}Cd, and ^{206}Pb), or by the method of standard additions (Mn and Co). The data from Zn, Cu, Ni, Cd, Pb, Mn, and Co will not be discussed in this manuscript. Samples were preconcentrated off-line using a home-built automated preconcentration unit. The basics of the system are similar to that described by Milne et al. (2010) except the flow pathway was all-Teflon with the peristaltic pump being replaced with a Teflon solenoid pump (130SP1230-1TP, Bio-Chem Fluidics). The system was controlled using custom-written software in LabVIEW (National

Instruments, Australia). Before preconcentration, samples were spiked with enriched isotopes of and an internal standard containing Sc, In, and Yb. Samples were equilibrated overnight. Prior to analysis, samples were buffered to a pH of ~7.2 with a clean 3-(N-morpholino)propansulfonic acid (MOPS) buffer and then preconcentrated onto Nobias Chelate PA1 resin (Biller & Bruland, 2012; Sohrin et al., 2008). Metals were eluted with 1 mol L^{-1} nitric acid and then determined by high resolution inductively coupled plasma–mass spectrometry (ICP-MS) (Element XR, ThermoScientific). Blanks and the detection limit for the iron are presented in Table S1. As a check on the precision and accuracy of the iron results, an in-house and external GEOTRACES intercalibration standards were run and found to be in good agreement with consensus values (Table S2).

For samples collected on the Australian leg, iron and supporting trace metals were determined by the method of standard additions. Samples were extracted and preconcentrated off-line using either (i) an in-house matrix separation and preconcentration manifold with Nobias-chelate PA1 resin (Queroue et al., 2014) or (ii) an ESI SeaFast system (Lagerström et al., 2013). Metals were eluted with 1 mol L^{-1} nitric acid and then determined by sector field ICP-MS with enhanced sensitivity (~10 times) using a capacitively coupling guard electrode (Element 2, ThermoFisher Scientific). Blanks and detection limits are presented in Table S3.

2.5. Rainwater Sampling

Ad hoc rainwater sampling was undertaken on the New Zealand leg. Samples were collected using a trace metal clean funnel fashioned from a 2 L linear low-density polyethylene bottle with the end removed (diameter: 110 mm). Samples were collected from the bow of the ship. After collection samples were acidified with nitric acid to $pH < 1.8$. Elemental concentrations for iron, zinc aluminum, copper, zinc, manganese, cadmium, and lead concentrations were determined directly by high-resolution ICPMS (Tables S4 and S5).

2.6. Aerosol Sampling

The concentration (nmol m^{-3} or pmol m^{-3}) and composition of both major and minor elements in aerosols was sampled on both ANZ voyages using a volumetric flow-controlled high-volume Lear-Siegler aerosol sampler (with total suspended particulate inlet) mounted on the ships superstructure above the bridge. Trace metal clean Whatman 41 filters were used, along with procedural blanks after Baker et al. (2016) and Martino et al. (2014). Sector control was set carefully to minimize any contamination from the vessels stacks. Air volumes sampled were typically ~1,300 m^3 over a 24 h sampling period while the ship was underway. The conversion from aerosol concentration to depositional flux was based on an atmospheric deposition velocity of 0.6 cm s^{-1} for elements predominantly associated with (>1 μm diameter) mineral dust (Fe, Al, and Mn) or 0.1 cm s^{-1} for elements associated with fine-mode (<1 μm diameter) aerosol particles (Zn, Cu, Ni, Cd, and Pb) (Table S6). Duce et al. (1991) estimated the uncertainty in the use of dry deposition velocities to be approximately a factor of 2–3.

2.7. Intercomparison of CTD, Nutrients, and Iron Data Sets at Crossover Stations

The CTD, nutrient, and iron concentration data sets between the two voyages were intercompared by collecting samples at two crossover stations on each of two voyages. Samples were collected between 15 and 1,500 m at 172°W, and 15 and 4,000 m at 170°W. The correlation between phosphate, nitrate, and silicate concentrations for samples collected at these two crossover stations was significant with regression slopes of 0.97 ± 0.02 ($n = 26$, $p < 0.001$), 1.00 ± 0.01 ($n = 26$, $p < 0.001$), and 1.07 ± 0.01 ($\mathrm{n} = 26$, $\mathrm{p} < 0.001$), respectively (Figure S2).

The correspondence between CTD-measured parameters was also significant for temperature, potential density, and dissolved oxygen, with regression slopes of 0.9949 ± 0.0008 ($n = 2045$, $p < 0.001$), 1.007 ± 0.0008 ($n = 2045$, $p < 0.001$), and 1.075 ± 0.001 ($n = 2046$, $p < 0.001$), respectively (Figure S2). The fluorescence measurements made using sensors on each CTD package on the two ANZ voyages were, however, significantly offset with a regression slope of 34.2 ± 1.0 and an $r^2 = 0.92$ ($p < 0.001$) between 0 and 200 m. To overcome this offset, the fluorescence data from the Australian voyage was normalized to the fluorescence data from the second voyage (NZ) across the depth range of 0 to 200 m at the two crossover stations.

The correlation for dissolved iron concentrations for samples collected at the two ANZ crossover stations was significant with a regression slope of 1.04 ± 0.09 ($p < 0.001$, $n = 22$, $r^2 = 0.92$) and an intercept of 0.03 ± 0.03 ($p = 0.39$, $n = 22$) (Figure S2).

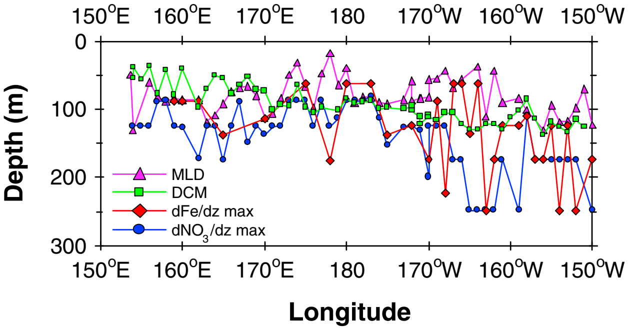

Figure 2. Depth of the mixed layer (MLD), deep chlorophyll maximum (DCM) (green), the nitracline (blue), and the ferricline (red). The nitracline and ferricline were calculated as the maximum change in concentration with respect to depth across a stratum between 50 and 500 m. The depth of the DCM is based on the fluorescence data from CTD profiles. The base of the mixed layer was defined as a change in density greater than $\Delta\sigma_\theta = 0.03$ kg m^{-3} (de Boyer Montégut et al., 2004).

The GP13 data presented here has been approved by the GEOTRACES Standards and Intercalibration Committee for inclusion in the second Intermediate Data Product released in August 2017.

2.8. N_2 Fixation Measurements

The methods used to determine N_2 fixation rates are based on those published by Law et al. (2012) and Montoya et al. (1996). Briefly, water was subsampled from Niskin bottles and pre-screened through a 200 mm mesh filter into 2.4 L acid-prewashed polycarbonate bottles (Nalgene). Samples were spiked with 2.5 mL of 99% ^{15}N enriched N_2 (Sigma Aldrich) injected into the bottle through a butyl rubber septum, followed by gentle reproducible agitation. Dissolved ^{15}N-N_2 concentrations were determined by analysis on a Membrane Inlet Mass Spectrometer. Samples were incubated at in situ temperature in temperature-controlled deck incubators at 20% PAR (photosynthetically active radiation). Incubations were terminated by filtration under low negative pressure on to 25 mm precombusted 0.7 μm GF/F filters (Whatman), with filters stored at −20°C. The background ^{15}N abundance for particulate nitrogen was determined by (a) immediate filtration at time zero, (b) control samples incubated with ambient air addition instead of ^{15}N-N_2, and (c) poisoned controls incubated with ^{15}N-N_2 and 1 mL mercuric chloride. Filters were dried and analyzed for ^{15}N uptake and incorporation into particulate organic nitrogen by stable isotope mass spectrometry using a NA1500 elemental analyzer (Fisons Instruments) interfaced to a Deltaplus (Thermo-Finnigan) continuous-flow isotope ratio mass spectrometer. N_2 fixation rates were determined as in Law et al. (2012), following the methods of Montoya et al. (1996).

2.9. Vertical Diffusivity, Ferricline, Nitracline, Phosphocline, and Flux Calculations

To provide an estimate of vertical diffusivity, given that only CTD profiles were available, an overturn scale approach was applied. While challenged by data paucity, the mixing estimates were concurrent with the chemistry data. As the bulk temperature profiles for each station for the GP13 voyage were monotonic in nature (Figure S3), a temperature-based Thorpe Scale approach could be applied. This approach used the raw temperature data from the CTD thermistors to detect overturn scales and then estimate turbulent diffusivity (Figure S4) (Finnigan et al., 2002; Stevens et al., 2014). This first identifies the overturn scale, estimates turbulent dissipation rate, and then, based on background stratification, estimates the diapycnal diffusivity (Osborn, 1980). The resulting estimates were aggregated into 50 m thick bins, over the top 500 m of the water column. In this analysis, downward velocity needed to be greater than >0.1 m s^{-1} for the entire segment for it to be acceptable, and only overturns greater than 0.25 m were considered. Electronic noise associated with the temperature sensors was very small compared to the signal, so in conjunction with the 0.25 m minimum overturn length scale, resulted in reasonable estimates. One issue encountered here, due the sparseness of the data, was that in some bins, total measured overturns only accounted for a proportion of the bin and so the final estimate had to be weighted accordingly. In addition, as identified in Osborn (1980) and subsequent studies, this must be regarded as an upper bound.

The depth of the ferricline, nitracline, and phosphocline were all calculated based on the maximum change in the dissolved iron (∂DFe/∂z), nitrate ($\partial NO_3/\partial z$), and phosphate ($\partial PO_4/\partial z$) concentration gradient below 50 m (Tagliabue et al., 2014). For flux calculations, we took the average of these gradients over the depth range from the base of the mixed layer to 500 m, which typically included three to five depths depending on the depth spacing across the depth range. Diffusion flux estimates for the supply of dissolved iron, nitrate and phosphate were calculated by multiplying the concentration gradient by diffusivity.

3. Results

3.1. Zonal Trends in Fluorescence, Dissolved Iron, and Nutrients

Across the ANZ (West to East) transect, a decrease in satellite-derived chlorophyll concentration is observed between 152°E and 150°W, indicating lower surface water phytoplankton biomass along the eastern part of the section compared to the west (Figure 1a). This east-west pattern is repeated subsurface where the DCM is

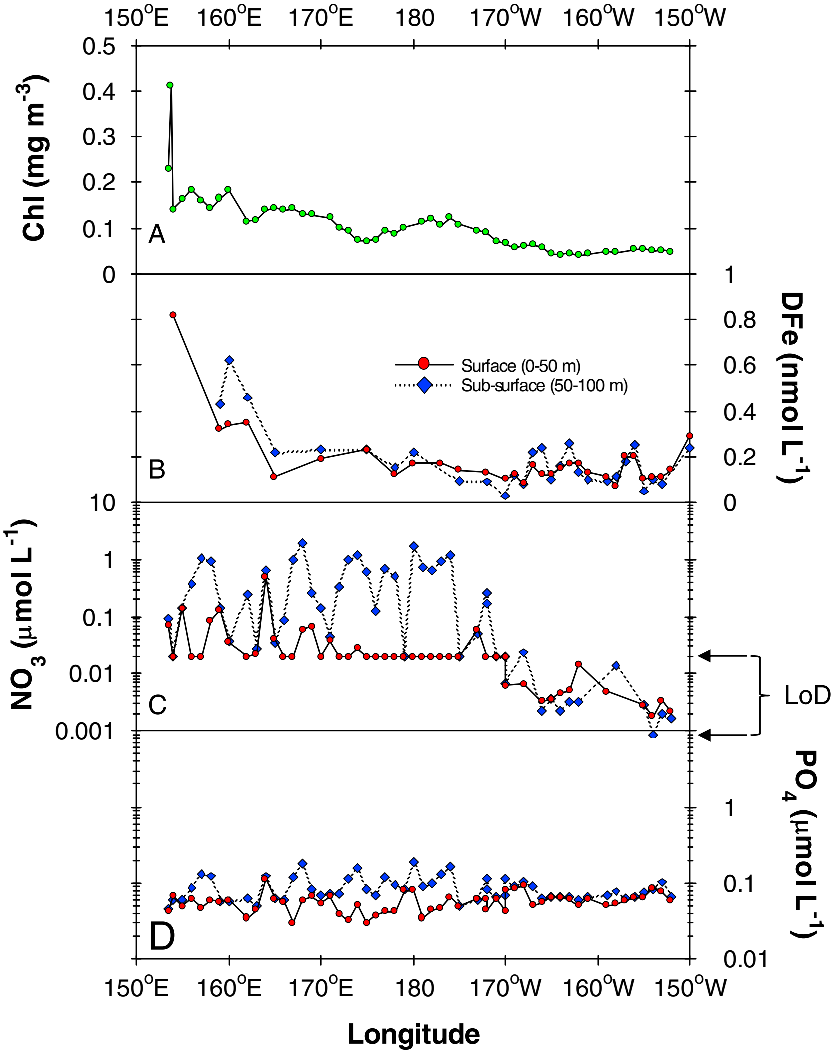

Figure 3. Surface (0–50 m) and subsurface (50–100 m) zonal transect data for (a) satellite-derived chlorophyll (surface only (upper 10 m); see Figure 1a), (b) dissolved iron, (c) nitrate, and (d) phosphate concentration. The nitrate concentrations from 170°W to 150°W are based on values determined using a nanonutrient system at selected stations. Black arrows on the side of Figure 3c represent the limit of detection (LoD) for the Australian (153°E to 170°W) and New Zealand (170°W to 150°W) voyages.

located at a shallower depth in the water column in the west (153–170°E, 61 ± 18 m) compared to the east (171–150°W, 106 ± 16 m) (Figures 1b and 2).

Surface (0–50 m) dissolved iron concentrations along the ANZ transect are generally low, ranging between 0.05 and 0.29 nmol L^{-1}, with an average of 0.15 nmol L^{-1} between 153°E and 150°W (Figures 3 and S5). Subsurface (50–100 m) iron concentrations followed a similar pattern. Along the ANZ section, east of 180°E, dissolved iron concentrations are also elevated by ~0.2 nmol L^{-1} above the background concentration of ~0.4 nmol L^{-1} between 1,500 to 3,500 m in low-oxygen NPDW (Figure 4). The elevated iron concentrations across this depth range appear consistent with the long-range transport (i.e., thousands of kilometers) of hydrothermally sourced iron for waters sourced north and east of the section (Fitzsimmons et al., 2014; Resing et al., 2015). Above and below this depth range, dissolved iron concentrations mostly ranged between 0.4 and 0.6 nmol L^{-1}.

Across northern New Zealand (170–180°E), dissolved iron concentrations are generally low in surface waters (~0.15 nmol L^{-1}), but higher at depth (Figures 4 and S5), again, suggestive of either continental or hydrothermal derived iron inputs associated with the Kermadec and Colville ridge systems. West of 165°E, dissolved

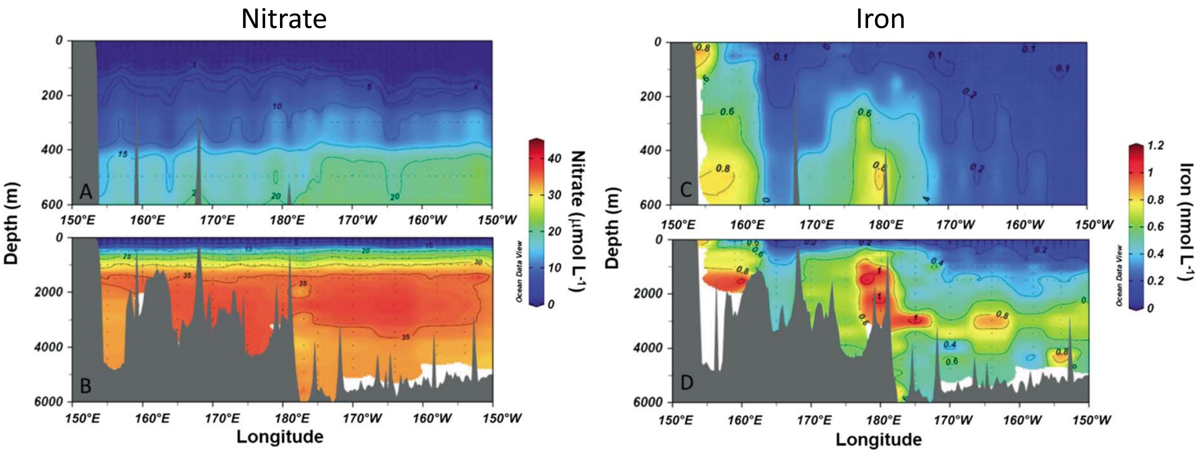

Figure 4. Longitudinal sections showing the distribution of (a, b) nitrate and (c, d) dissolved iron for the upper water column (0–600 m) and the full water column (0–6,000 m).

iron concentrations are elevated in surface waters, especially at stations close to continental Australia (Figures 3 and 4), consistent with atmospheric iron inputs associated with the eastward transportation of dust from the Australian interior and continental margin supply (Figure 5) (Ellwood et al., 2013; Gabric et al., 2016; Mackie et al., 2008).

The surface (0–50 m) inventory of nitrate also declined from west to east, matching the zonal trend of declining satellite-derived chlorophyll concentration along the ANZ section (Figures 3 and S6). East of 170°E, the nitrate concentration in the upper 50 m was at or below 20 nmol L^{-1} (Figure 3). A similar trend of very low nitrate concentration has been observed during summer in the North Tasman Sea at ~30°S; 172°E (Ellwood et al., 2013; Law et al., 2011) indicating that this region is oligotrophic year round, with respect to nitrate. The half-saturation (Ks) constant for nitrate uptake from oceanic waters varies between about 20 and

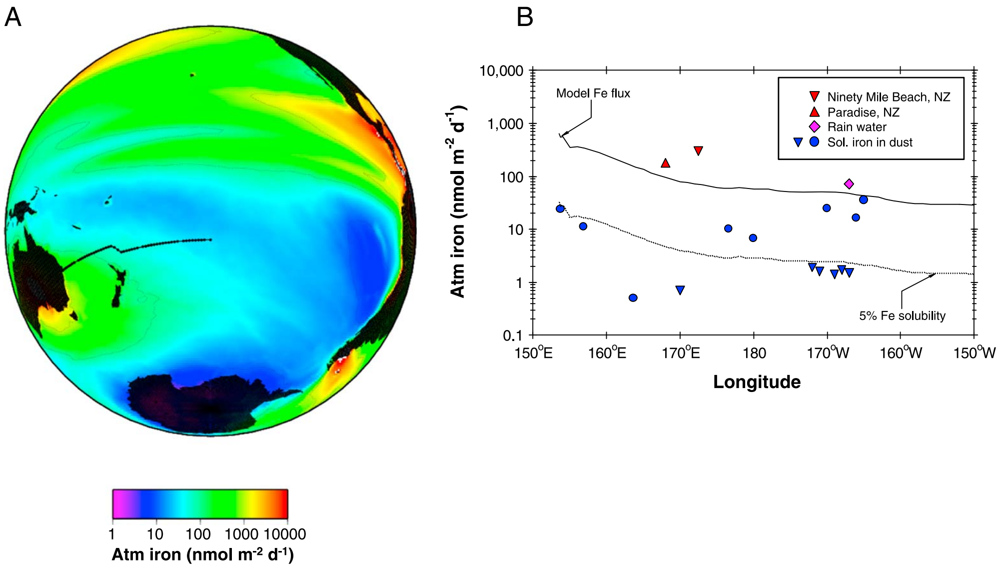

Figure 5. (a) Annual mean atmospheric iron deposition flux data. Dust data were extracted from the Albani et al. (2014) model and converted to an iron deposition flux by assuming 3.5% w/w iron. (b) Atmospheric iron deposition flux for the ANZ section extracted from Albani et al. (2014) model dust data set and converted to an iron flux (as in Figure 2a). Dotted line assumes 5% of the atmospheric iron flux from the model data set is soluble. Overlayed are soluble iron flux measurements for dust samples collected on the ANZ section (blue dots and inverted triangles) and rainwater data (total dissolvable iron) for samples obtained on the NZ leg section (Table S7). Also shown are iron deposition data for the SW Pacific Ocean from New Zealand (Arimoto et al., 1987; Halstead et al., 2000). Inverted blue triangles represent samples at the limit of detection for the measurement of the soluble iron flux (Table S7).

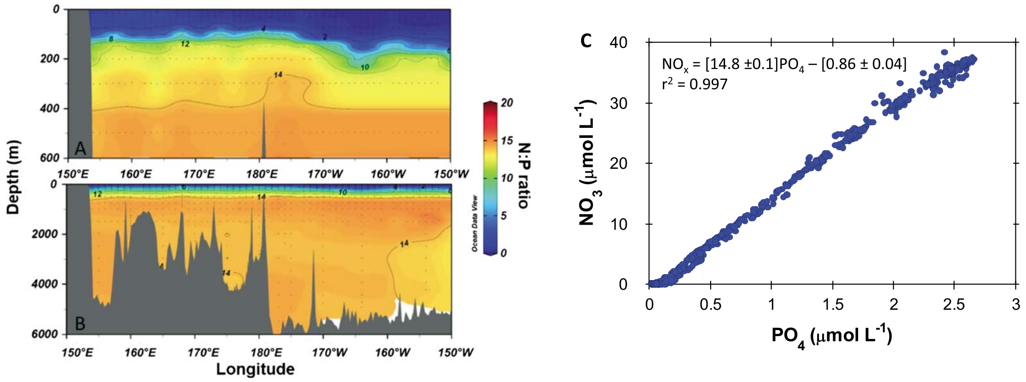

Figure 6. (a, b) Longitudinal sections showing the N:P ratio for the upper water column (0–600 m) and the full water column (6–6,000 m). (c) Plot of nitrate concentration versus phosphate concentration for water column samples collected along the GP13 section.

30 nmol L^{-1} (Harrison et al., 1996); thus, chronic nitrate limitation of phytoplankton along the GP13 transect might be expected as background concentrations typically well below Ks values as observed by Law et al. (2011), Raimbault et al. (2008), Bonnet et al. (2008), and Ellwood et al. (2013). In contrast, phosphate concentrations (0–50 m) along the ANZ section varied within a narrow range of between 30 and 110 nmol L^{-1} (Figure 3) and exceed concentrations ($<$ 15 nmol L^{-1}) regarded as phosphate limiting for phytoplankton (Kretz et al., 2015; Moore et al., 2013).

Nitrate concentrations increased with depth with higher levels in AAIW (500–1,000 m), and LCDW ($>$4,000 m) compared to that of the surface (Figures 4 and S6). The highest concentrations are observed with North Pacific Deep Water (NPDW, 1,500–3,000 m) along the eastern part of the section (Figures 4 and S1). These hydrographic differences were also reflected in the oxygen content of these different water masses with recently ventilated AAIW and LCDW/AABW having a higher dissolved oxygen concentration compared to NPDW/UCDW (Figure S7).

3.2. Vertical Iron and Nutrient Concentration Gradients

The depth of the ferricline is generally shallower (average = 103 ± 37 m; range: 62 to 175 m) but generally within 20–50 m of the mixed layer depth (MLD) along the western part of the ANZ section (153°E to 170°W). The ferricline deepened significantly (average = 139 ± 61 m; range: 62 to 248 m, $p < 0.04$) across the eastern end of the section (170°W to 150°W) and is approximately 60 m deeper than the MLD (Figure 2).

Like iron, the depth of the nitracline is generally shallower (average = 117 ± 25 m; range: 80 to 175 m) along the western part of the ANZ section (153°E to 170°W), and deepened (average = 149 ± 54 m; range: 80 to 248 m, $p < 0.01$) across eastern end of the section (170°W to 150°W) (Figure 2). Between 153°E and 170°E and 170°W and 150°W the depth of the nitracline is slightly deeper than that of the ferricline, whereas between 170°E and 170°W the depth of the nitracline and the ferricline coincided (Figure 2).

The depth of the phosphocline is also closely associated with that of the nitracline along the entire section (data not presented). Nitrate and phosphate concentrations are strongly coupled zonally along the section with an N:P slope of 14.8 ± 0.1 ($r^2 = 0.997$) (Figure 6).

The dissolved iron concentration gradient between the base of the mixed layer and 500 m ranged between 0.19 and 2.88 nmol m^{-4}, with an average of 1.13 ± 0.69 nmol m^{-4} (Figure 7). The dissolved iron concentration gradient decreased eastward with lower values occurring between 170°W and 150°W. The nitrate concentration gradient between the base of the mixed layer and 500 m ranged between 24 and 108 µmol m^{-4} with an overall average of 51 ± 14 µmol m^{-4} (Figure 7). There appears to be a potential maximum in the nitrate gradient between 170°E and 170°W after which the gradient appears to decline between 170°W and 150°W. The phosphate concentration gradient between the base of mixed layer and 500 m ranged between 0.92 and 7.97 µmol m^{-4} with an overall average of 3.23 ± 0.92 µmol m^{-4} (Figure S8). There is a strong coupling between the nitrate and phosphate gradients where the nitracline and phosphocline coincide. The N:P ratio is 16 ± 3 (n = 43) at the depth of the nitracline and phosphocline. Similarly, there is also a strong coupling

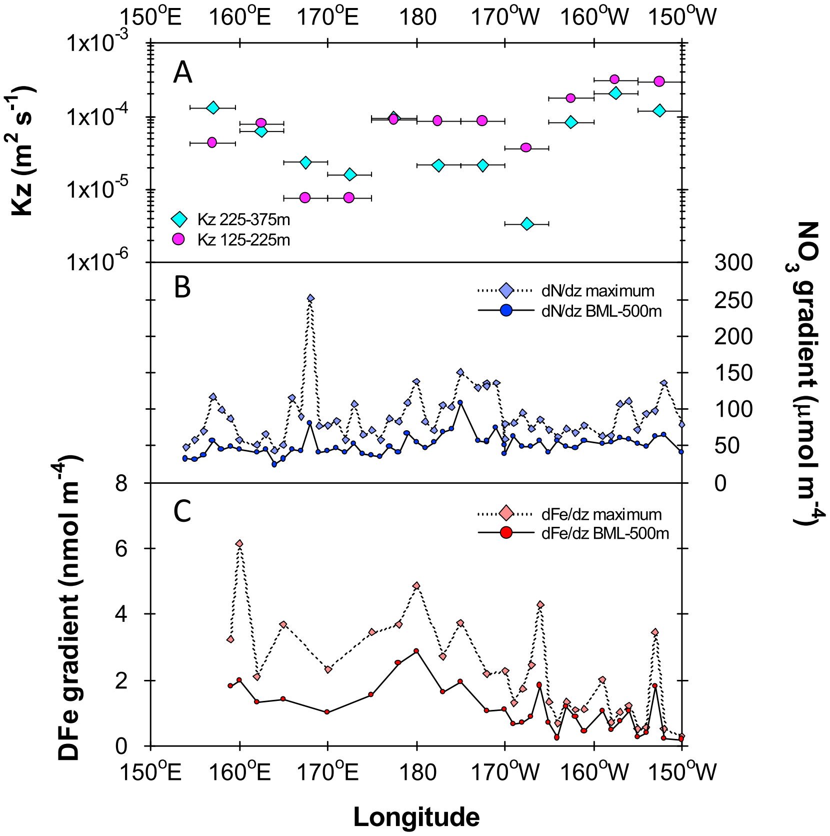

Figure 7. Section results for (a) diffusivity (Kz) across 125–225 m and 225–375 m binned to 5° of longitude, (b) dissolved nitrate (blue), and (c) dissolved iron (red) concentration gradients across a depth range between the base of the mixed layer (BML) to 500 m. Presented in Figures 7b and 7c are the average and the maximum values across the depth range.

between average nitrate and phosphate gradient between the base of mixed layer and 500 m with a N:P ratio of 16 ± 3 (*n* = 43).

We observed a local minimum in dissolved iron concentration at depth at several stations. The depth of this minimum varied and coincided with the depth of the DCM for only some of the stations (Figure 8). This minimum in dissolved iron concentration at the DCM has been observed for regions with high dust flux inputs, such as in the Sargasso Sea and the North Pacific Ocean (Boyle et al., 2005; Bruland et al., 1994; Hatta et al., 2015; Sedwick et al., 2005) and has been attributed to biological uptake, perhaps reflecting an increased iron requirement of light limited phytoplankton (Hopkinson & Barbeau, 2008) and/or scavenging of iron post atmospheric input.

3.3. Aerosol Inputs of Iron and Nitrogen Species

Measured input fluxes for aerosol iron are presented in Figure 9c. The aerosol inputs of dissolved iron is variable with flux values ranging between 0.5 and 36 nmol m^{-2} d^{-1}. To complement these measured fluxes, we estimated the supply of iron from the atmosphere across the ANZ transect by incorporating model calculations of dust deposition across the South Pacific (Figure 9c) (Albani et al., 2014). To converted model dust-derived iron deposition values into a soluble iron supply flux, we assigned an iron solubility of 5%, which compares well to the measured soluble iron fluxes insofar as the relative ranges for the two datasets are similar (Figure 5b and Text S1). It should also be noted that during the New Zealand leg the Puyehue-Cordón Caulle volcanic complex erupted (4 June 2011) and ejected significant amounts of ash into the atmosphere (Draxler & Hess, 1998; Nakamae et al., 2014; Stein et al., 2015) (Figure S9 and Text S2), which might explain the variability in the measured soluble iron fluxes east of 170°W (Figure 5b) (Rogan et al., 2016). Volcanically sourced iron tends to be more soluble as it is usually processed with volcanically derived acids (Ayris & Delmelle, 2012). The measured and model-derived fluxes here are consistent with values obtained for the

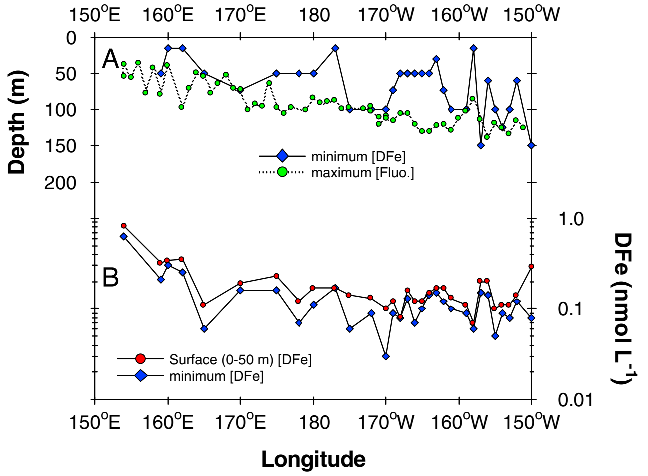

Figure 8. (a) Depth at which the maximum in chlorophyll fluorescence (DCM) and the minimum in dissolved iron concentration occur for measured profiles. (b) Average dissolved iron concentration between 0 and 50 m and at the depth minimum. Note that dissolved iron concentrations are expressed on a log scale.

South Pacific basin across similar latitudes (Figure 5 and Table S5) (Arimoto et al., 1987; Buck et al., 2013; Halstead et al., 2000). Soluble nitrogen aerosol input fluxes calculated for samples collected between 172°W and 165°W ranged between 25 and 237 nmol m^{-2} d^{-1} for ammonia and 328 and 1284 nmol m^{-2} d^{-1} for nitrate (Figure 9f). These values are consistent with values obtained by Martino et al. (2014) for the Southwest Pacific Ocean.

3.4. N_2 Fixation Measurements

Nitrogen fixation rates measured for surface waters between 170°W and 150°W are low and averaged 0.036 ± 0.016 nmol L^{-1} d^{-1} (Figure 9f). These values are lower than the rates obtained made by Halm et al. (2012) at a three stations along a similar longitude (0.12–1.16 nmol L^{-1} d^{-1}) during the 2006/2007 austral summer and also for the northern Tasman Sea at corresponding latitudes (Figure 9f) (Law et al., 2011, 2012).

3.5. Vertical Diffusivity Estimates

The vertical diffusivities (Kz) values estimated in this study varied considerably with minimum estimate values ranging between 7.5×10^{-6} and 3.1×10^{-4} m^2 s^{-1} (Figures 7 and S4). These values are comparable to the value (~1×10^{-4} m^2 s^{-1}) obtained by Stevens et al. (2012) for the North Tasman Sea (~30°S; ~171°E) and within the range measured by Law et al. (2001, 2003) using sulfur hexafluoride labeled experiments, but are generally higher than canonical values 1–4 × 10^{-5} m^2 s^{-1} (Ledwell et al., 1993; Lewis et al., 1986), which represent main thermocline

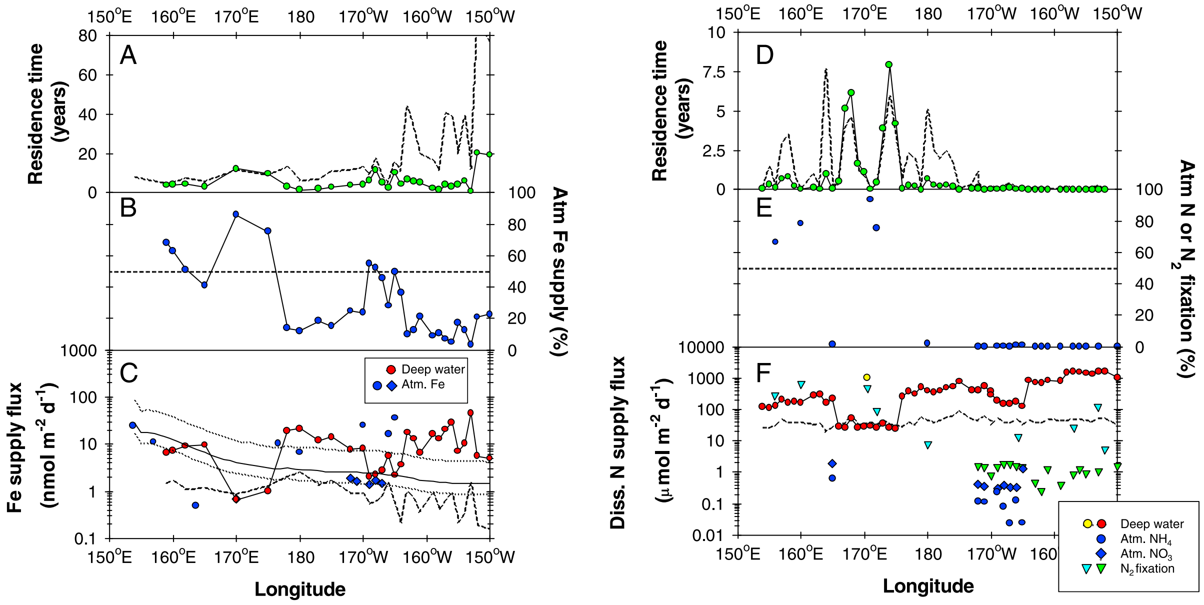

Figure 9. (a) Residence time of dissolved iron in the upper ocean (0-MLD). (b) Estimates of the relative proportion of atmospheric supplied iron into surface waters (0-MLD) versus that of the diffusive supply of iron from depth. (c) Measured dissolved iron flux for iron supplied via the atmosphere (blue dots and diamonds) and iron supplied via diffusion from the deeper ocean (red circles). (d) Residence time of dissolved nitrate in the upper ocean (0-MLD). (e) Estimates of the relative proportion of nitrogen supplied from depth relative to nitrogen fixed and atmospherically fixed nitrogen. (f) Dissolved nitrogen supplied via diffusion from the surface mixed layer (red and yellow circles), nitrogen fixation (green and teal inverted triangles), and supplied from the atmosphere (blue circles, squares and diamonds). The dashed line in Figures 9a and 9d represents residence times based on a Kz value of 1×10^{-5} m^2 s^{-1} (Ledwell et al., 1993). Likewise, the dashed line in Figures 9c and 9f represents a lower diffusion supply estimate based on the Kz value from Ledwell et al. (1993). The solubility of the atmospheric iron was assumed to be 5% with the dotted lines representing solubilities of 3 and 15%, respectively, in Figure 9c (Chance et al., 2015; Desboeufs et al., 2014; Powell et al., 2015). The data in each panel were either from this study or from Law et al. (2011, 2012), Halm et al. (2012) (teal inverted triangles), Martino et al. (2014) (blue circle and diamond at ~165°E) and Stevens et al. (2012) (yellow circle).

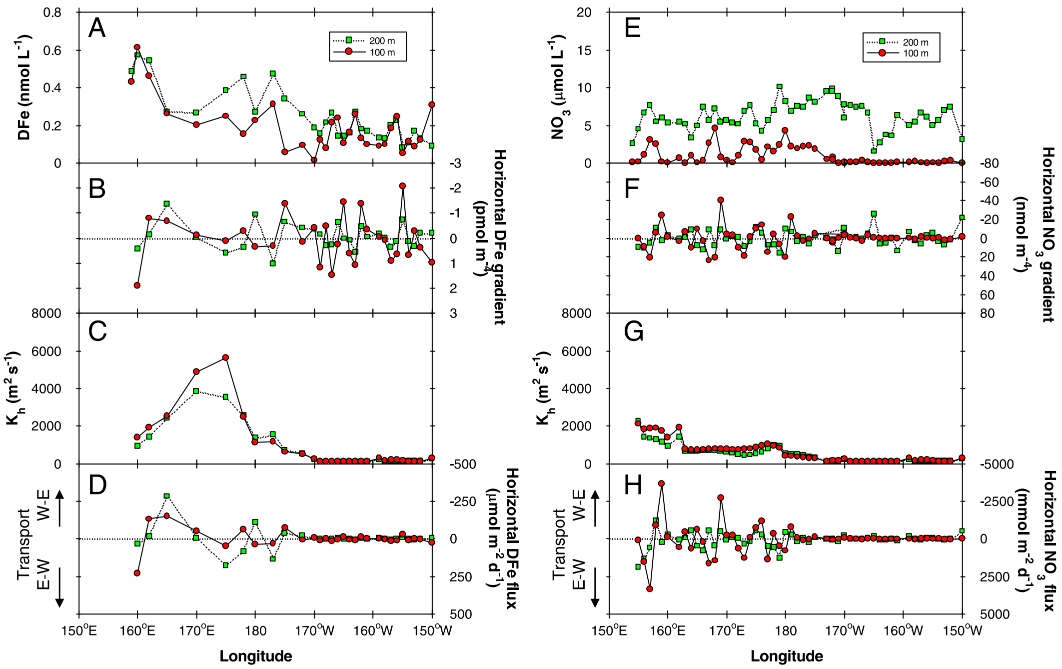

Figure 10. Zonal results for (a) dissolved iron concentration at 100 m and 200 m, (b) horizontal dissolved iron gradient at 100 m and 200 m, (c) horizontal diffusivity at 100 m and 200 m, (d) horizontal dissolved iron flux, (e) nitrate concentration at 100 m and 200 m, (f) horizontal nitrate gradient at 100 m and 200 m, (g) horizontal diffusivity at 100 m and 200 m, and (h) horizontal nitrate flux. Negative flux values indicate diffusion from west to east, while positive flux values indicate diffusion from east to west. Horizontal diffusivities were extracted from the 100 m and 200 m depth intervals in 3° × 3° gridded data set presented by Cole et al. (2015) and interpolated to individual station positions; that is, Kh varies with the distance between stations, hence the variation in individual Kh values.

values; thus, the Kz estimates from these two studies can be regarded as a lower limit. The Kz estimates for the present study are binned to 5° of longitude and then used (125–225 m depth stratum) in the calculation of the diffusive supply flux for dissolved iron, phosphate, and nitrate into the upper ocean. The GP13 Kz estimates are subject to considerable uncertainty due to spatial-temporal variability in processes driving the vertical mixing.

3.6. Horizontal Supply Estimates

Cross-frontal exchange and horizontal transport can play a role in nutrient supply in subtropical regions (Letscher et al., 2016; Lewis et al., 1986; Palter et al., 2013). We observed a zonal gradient in dissolved iron concentration between 158°E and 180°, which is associated with continental margin and underwater features (Figure 10). However, the zonal supply gradient (west-east, 100 m to 200 m) for dissolved iron (range: -2.1 to 1.9 pmol m^{-4}) are approximately 3 orders of magnitude lower than the vertical supply gradient for dissolved iron (range: 0.13 to 2.62 nmol m^{-4}). That said, dissolved iron concentrations between 158°E and 170°E decreased in an exponential-like manner, thus presenting a horizontal gradient with a likely continental shelf source (Figure 10) (Fitzsimmons et al., 2016; Rijkenberg et al., 2012). This is supported by the general structure of the dissolved iron profiles in this region (158°E and 170°E), which exhibited higher concentrations between 200 m and 600 m compared to profiles collected further east along the transect (e.g., 160°W and 150°W) (Figure S5).

To estimate the zonal flux supply of iron, we multiplied the horizontal dissolved iron concentration gradient by horizontal diffusivity estimates extracted from the data set of Cole et al. (2015) which are based on Argo float observations. We are conscious that horizontal diffusivity is a function of length scale (Okubo, 1971). Horizontal diffusivities in Cole et al. (2015) were computed at 3 × 3° resolution, whereas our resolution between stations is on the order of 1°. Using a 1° resolution leads to an over estimation of the horizontal diffusivity by about a factor of 4. We corrected for this by scaling horizontal diffusivities to the distance between stations (Okubo, 1971) (Figures 10 and S10). We restricted our calculations to 100 m and 200 m as below these depths SAMW and AAIW dominate with meridional flow paths (Figure S7). Using this approach, we estimate that there is some eastward fluxing of iron into the north Tasman Sea (158°E and 170°E) (Figures 10 and S10) and between 175°W and 170°W with potential sources from continental Australia and the Kermadec Ridge, respectively. Apart from these two regions, there is no apparent trend in the horizontal iron flux data with averages of 2 ± 13 μmol m^{-2} d^{-1} and −1 ± 4 μmol m^{-2} d^{-1} between 170°W and 150°W for 100 m and 200 m, respectively. These averages are statistically the same as zero implying that diffusive horizontal transport appears to be low outside of the aforementioned regions.

In contrast to iron, there is no evident shelf input of nitrate thus variations in the horizontal nitrate concentration gradient across the GP13 section are low. The horizontal zonal gradient for nitrate (west-east, 100 and 200 m) ranged between −14 and 26 nmol m^{-4}, approximately 3 orders of magnitude lower than the vertical supply gradient for nitrate (31 to 252 μmol m^{-4}) (Figure 10).

4. Discussion

Across the Subtropical South Pacific Ocean, the supply of nitrogen into the euphotic zone appears to be the key control on biological nondiazotroph production, with potential secondary limitation by iron and phosphate supply via their influence on diazotroph production (Bonnet et al., 2008; Ellwood et al., 2013; Moisander et al., 2012; Raimbault et al., 2008; Shiozaki et al., 2014; Wagener et al., 2008). Here we discuss the zonal distribution of iron, nitrate and phosphate across the ANZ transect and investigate the likely sources and cycling and their relative roles in controlling biological production, with respect to the biogeochemical provinces outlined by Ward et al. (2013).

4.1. Iron Supply Into the Upper and Deeper Ocean

The main sources for dissolved iron in the euphotic zone are from the vertical diffusion from the deeper ocean and atmospheric supply with some horizontal sourcing of dissolved iron into the upper thermocline (100–200 m) between 158°E and 170°E and 175°W and 170°W. Outside of these regions horizontal iron supply gradient appears to be small.

By combining vertical dissolved iron concentration gradients and vertical diffusivities, we are able to develop estimates of the upward diffusive dissolved iron flux to remote South Pacific surface waters (Figure 9c). These calculations complement the atmospheric supply fluxes presented in Figure 5. Based on the relative portion of these supply estimates, we find that the vertical diffusion flux represents approximately 77 ± 17% of the total source flux iron into the surface ocean east of 170°W, even though the diffusive flux declined eastward and despite considerable variability in the Kz values used to calculate the diffusive iron supply flux (Figure 7a). As mentioned, the Kz values estimated for ANZ zonal section are elevated relative to values obtained by Ledwell et al. (1993). If the Kz values from Ledwell et al. (1993) are used to calculate the diffusive iron flux relative to the atmospheric iron flux, then the contribution of dissolved iron delivered into the euphotic zone via diffusion is 36 times lower (Figure 9). For waters, west of 170°W the sourcing of dissolved iron into the upper thermocline (100–200 m) occurs in the north Tasman Sea (158°E and 170°E) and near the Kermadec Ridge, system and will help surface ocean iron resupply by elevating concentrations within the thermocline.

Our calculations indicate that atmospheric iron supply contributes 23 ± 17% of the total dissolved iron input into the upper ocean between 170°W and 150°W. This is a somewhat surprising result considering that the atmospheric iron flux declines by about tenfold between 153°E and 150°W (Figures 5b and 8c). Initially, we had anticipated that deep water iron supply would dominate in these waters because they are relatively remote with respect to a continental dust input sources (Li et al., 2008) (Figures 5 and 10). Notwithstanding, the supply of atmosphere iron still appears to be a significant source to the upper ocean away from continental sources (Figure 9b). This raises the notion as to whether dissolved iron within the thermocline reflects iron that has been sourced from the atmosphere but has subsequently dissolved either in the surface ocean or has sunk to depth and then dissolved.

To probe this idea further, we looked at the underlying water masses and their potential to supply iron into the euphotic zone using the Wu and Boyle (2002) pipe model. This model incorporates scavenging and remineralization processes for dissolved iron within a water parcel during long-distance transits along an isopycnal surface. The main water masses that dominate the thermocline across the zonal section are SAMW and AAIW. Both water masses originate in the Southern Ocean and typically have a dissolved iron concentration near their formation region of approximately 0.1–0.15 nmol kg^{-1} (Bowie et al., 2009; Ellwood et al., 2008). The transit time it takes for these water masses to transit from the Southern Ocean will vary with latitude; however, based on anthropogenic radiocarbon invasion, the transit time for AAIW to reach at 150°W is on the order of 33 years (Jenkins et al., 2010). Using this information and combining it with the dissolved iron concentration for SAMW/AAIW at 150°W (~0.24 nmol kg^{-1} at 750 m), we can calculate a regenerative iron concentration flux using the pipe model (Wu & Boyle, 2002). The equation for this model is as follows

$$\frac{\mathrm{d[Fe]}}{\mathrm{d}t} = F - k[\mathrm{Fe}] \tag{1}$$

where the change in dissolved iron concentration along an isopycnal surface, such as for SMAW and AAIW, is dependent on the input concentration flux (F, nmol kg^{-1} yr^{-1}), for iron regenerated from sinking particulate material, minus the rate for dissolved iron scavenging (k, $year^{-1}$) from solution multiplied by the dissolved iron concentration [Fe]. Integration of equation (1) produces

$$F = \frac{k[\mathrm{Fe}] - k[\mathrm{Fe}]_0 e^{-kt}}{1 - e^{-kt}} \tag{2}$$

where $[\mathrm{Fe}]_0$ represents the original dissolved iron concentration for AAIW. Assuming a k value between 0.005 $year^{-1}$ and 0.01 $year^{-1}$ (Wu & Boyle, 2002), the change in the dissolved iron concentration in AAIW after 33 years of transit would be -0.03 nmol kg^{-1} assuming an initial concentration ($[\mathrm{Fe}]_0$) of 0.10 ± 0.05 nmol kg^{-1} is sourced from waters south of New Zealand (Ellwood et al., 2008) but with no regenerative inputs associated with sinking particulate matter. This reduction in [Fe] highlights the change in the dissolved iron concentration associated with scavenging. In contrast, the measured dissolved concentration at 150°W at 750 m is 0.24 ± 0.05 nmol kg^{-1}; thus, an addition 0.17 ± 0.05 nmol kg^{-1} of dissolved iron is required and this must be sourced from particulate matter sinking as it transits from the Southern Ocean to 150°W. To increase the concentration of dissolved iron to 0.24 nmol kg^{-1} requires a particulate iron regeneration flux of approximately 6.0 ± 2.9 pmol L^{-1} yr^{-1}. The atmospheric flux of soluble iron at 150°W is estimated to be approximately 1.45 nmol m^{-2} d^{-1} (or 0.53 μmol m^{-2} yr^{-1}) based on the model data from Albani et al. (2014) (Figure 5). Assuming that this atmospherically sourced iron becomes incorporated into organic matter and eventually sinks to depth, we can estimate the amount that is likely to be regenerated into SAMW/AAIW by applying a power law fit to model its vertical attenuation (a Martin-type regeneration function (Martin et al., 1987)). Using this approach, a regenerative iron flux of 0.07 pmol L^{-1} yr^{-1} at 750 m is obtained using a b-factor of -0.13 for iron (Boyd et al., 2017). This value represents approximately 1% of the flux required to balance the pipe model estimates. Clearly, there are caveats associated with these calculations—for example, dust solubility, the vertical attenuation factor, and the potential for sinking dust particles to dissolve subsurface—however, they do suggest that atmospheric iron at 150°W is not a major source to SAMW/AAIW. Rather, the source of iron to these water masses would appear to reflect an accumulation of dissolved iron from sinking material along the SAMW/AAIW flow path. That said, the surface ocean does appear to be influenced by atmospheric iron inputs consistent with the findings of Wagener et al. (2008) (Figure 9).

Implicit in this discussion is organic complexation of dissolved iron by natural organic ligands. Ligands are important in regulating iron retention, particle dissolution, and iron loss from solution (Boyd & Tagliabue, 2015; Fishwick et al., 2014; Hassler et al., 2017; Völker & Tagliabue, 2015). Background ligand concentrations measured at a limited number of stations averaged 2.20 nmol L^{-1} (range 0.67 to 14.7 nmol L^{-1}; 0–1,000 m) indicating that ligand concentrations exceed background dissolved iron concentrations.

Using both the atmospheric and diffusional iron supply fluxes, the residence time for dissolved iron within the upper ocean (0–100 m) across the zonal section (Figure 9a) can be computed (it should be noted that these residence time estimates do not account for the supply of iron from dissolution of the upper ocean resident particulate iron pool, or from lateral advection; thus, these times may be slightly overestimated). The residence time of dissolved iron from the 0 m to the base of the mixed layer averaged 4 years (range 1.4 to 12 years) between 153°E and 170°W and increased to ~20 years near the eastern end of the section (Figure 9). It should be noted that the residence time calculations are based on the Kz values presented in Figure 7; if we use the canonical value from Ledwell et al. (1993) of 1×10^{-5} m^{-2} s^{-1}, residence times for iron increase significantly by about a factor of 4. The general west-east increase in the residence time of iron in the upper ocean likely reflects a decrease in both the dissolved iron supply flux from deeper waters and a reduction in the atmospheric deposition of iron to surface waters. Coupled with these decreases, we speculate that iron is likely to be efficiently recycled by the resident plankton communities within and above the DCM. A typical *fe*-ratio for iron cycling in remote low dust source waters is on the order of 0.1 or less (Boyd et al., 2017; Landry et al., 1997). The production of iron binding ligands will also help keep iron in solution by reducing the chance of loss through scavenging processes (Fitzsimmons et al., 2015). Efficient iron recycling and organic complexation will help to increase the residence time of dissolved iron within the surface ocean.

The residence times calculated here for dissolved iron are higher than those estimated for waters where there is high seasonality in dissolved iron concentrations (Fitzsimmons et al., 2015); for example, dissolved iron in the waters near Hawaii has a residence time of approximately 0.5 years and in the Equatorial Atlantic it has a residence time between 0.5 and 10 years (Boyle et al., 2005; Croot et al., 2004; Fitzsimmons et al., 2015). Likewise, the residence times calculated in this study are much longer than those estimated from export fluxes during the subtropical FeCycle II study (east of New Zealand) where dissolved iron is being actively drawn down and exported from the surface ocean during the evolution of a springtime phytoplankton bloom (Ellwood et al., 2014). In the FeCycle II study, residence times for dissolved iron ranged between 1 and 206 days and varied depending on the phase of the bloom. The residence times calculated for dissolved iron across the ANZ zonal section are orders of magnitude higher compared to FeCycle II estimates, highlighting the oligotrophic nature of the South Pacific Ocean.

4.2. Nitrogen Supply into the Upper Ocean

Using the diffusional flux for nitrate, the atmospheric depositional rate for nitrogen species, and the surface water nitrogen fixation rate for the section, we estimated the relative contribution to each nitrogen supply source into the euphotic zone (Figure 9f). As we lack atmospheric deposition data for the western section of the transect, we have supplemented this with data from Martino et al. (2014) and nitrogen fixation data from the PINTS, NCycle, and COST campaigns (Law et al., 2011, 2012). The atmospheric deposition flux of soluble nitrogen species across the section is relatively low (typically less 2 μmol m^{-2} d^{-1}), whereas rates for nitrogen fixation from the PINTS, NCycle, and COST voyages are elevated in the western part of the section in comparison to the rates along the eastern GP13 section measured during this study (Figure 9f).

The upward diffusive flux of nitrate represents a significant source of nitrogen into the euphotic zone (Figure 9f). Between 170°W and 150°W, the diffusional supply of nitrate into the euphotic zone represented >98% of the total source flux into the surface ocean. In contrast, along the western part of the section, the diffusional supply of nitrate into the euphotic zone ranged between 28 and 99% of the total source flux (Figure 9e). If the Kz value of Ledwell et al. (1993) is applied, the diffusional supply of nitrate into the euphotic zone between 170°W and 150°W still dominates (>96%), whereas along the western part of the section nitrogen fixation becomes an even more important supply flux. Based on these results, it would appear the upward diffusive flux of nitrate into the euphotic zone is the primary supply of nitrogen to fuel new production east of about 175°E.

In contrast to iron, the residence time of dissolved nitrate from 0 m to the base of the mixed layer is much shorter with an average of 248 days (range 1.2 to 2,887 days) (Figure 9d). There are clear peaks in nitrate residence time between 165°E and 180°W, suggesting a reduction in the rate of nitrate supply into the euphotic zone. These peaks in the residence times for nitrate tended to occur when Kz values are at a minimum (Figure 7a). This is particularly obvious when the Kz value of Ledwell et al. (1993) is applied; residence times can be up to nine times higher. The shorter residence time of nitrate relative to that of iron is somewhat strange as iron has a longer regeneration length scale compared to that of nitrogen (Boyd et al., 2017; Twining et al., 2014). The longer residence time of iron relative to nitrate may relate to is complexation to natural organic ligands. Additionally, it may also indicate that nitrogen is taken up and exported from the euphotic zone on a much shorter timeframe compared to that of dissolved iron, i.e. iron is more efficiently recycled. This needs to be explored further.

4.3. Phosphate Supply Into the Upper Ocean

The supply of phosphate into the euphotic zone covaried with that of nitrate. The N:P ratio at the depth of the nitracline and phosphocline is 16 ± 3, which is statistically the same as the deep water (>500 m) N:P ratio of 14.5 ± 0.5. Interestingly, the N:P ratio in surface waters (0–50 m) is much lower with an average of 0.6 ± 0.7.

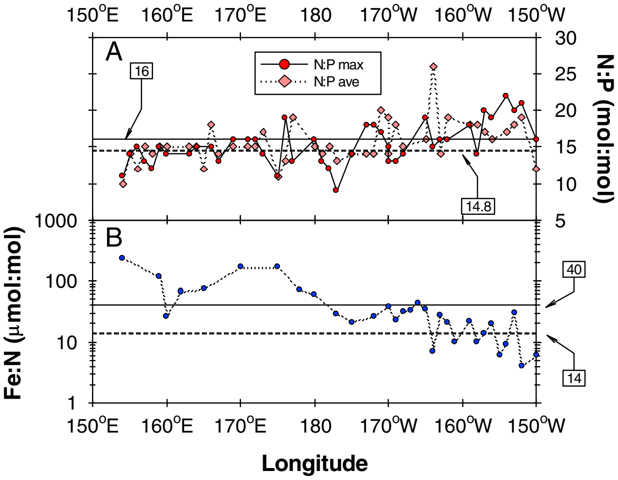

Figure 11. (a) Nitrogen to phosphorous ratio for the supply of these two nutrients into the euphotic zone via diffusional and atmospheric supply processes. (b) Iron to nitrogen ratio for soluble iron and nitrogen supplied into the euphotic zone via diffusional and atmospheric supply processes. Call out values in Figure 11b represent optimum and minimum Fe:N ratios for phytoplankton growth. Values taken from Moore et al. (2004, 2013).

This decline in the N:P ratio is similar to that observed by Raimbault et al. (2008) for South Pacific gyre and would suggest either that the assimilation ratio of N:P by phytoplankton in the euphotic zone is higher than 16 or that nitrate is being lost via denitrification. It is unlikely that denitrification is occurring as surface and sub-surface waters are well oxygenated (Figure S7); thus, it would appear that nitrate assimilation is the cause for the decline in the N:P ratio. Without measurements of nitrite, ammonia and nitrous oxide concentrations and rates of exchange between nitrogen species, we can only speculate as to the cause of the faster depletion of nitrate relative to that of phosphate in surface waters.

Phosphate star (P*) values calculated (where $P^* = PO_4 - NO_3/14.5$) for surface waters (0–50 m) are positive and ranged between 0.028 and 0.099 nmol L^{-1}, with an average of 0.056 ± 0.016 nmol L^{-1} (Note that these values may be an underestimate as some values are at the limit of NO_3 detection). These *P** values are consistent with increased assimilation of nitrate relative to that of phosphate resulting in residual phosphate accumulation in surface waters. The diffusional flux for phosphate supply into the euphotic zone ranged between 2 and 98 μmol m^{-2} d^{-1}. These values are about 100- to 1,000-fold higher than the atmospheric deposition of phosphate in the South Pacific region (Martino et al., 2014). Thus, it appears the primary supply vector for phosphate into surface waters in the South Pacific region is from diffusional supply from deep water. The residence time of phosphate in the surface ocean (0-MLD) is higher than that of nitrate as a result of its larger inventory within euphotic zone with values ranging between 0.17 and 17 years (Figure S11).

4.4. Insights in South Pacific Biogeochemistry: The Roles of N:P:Fe Stoichiometry on Biological Production

Using the dissolved iron and nitrate supply fluxes, the Fe:N supply ratio in the euphotic zone can be calculated (Figure 11). Across the entire ANZ section the Fe:N supply ratio ranged between 4 to 238 μmol:mol with an average of 47 ± 55 μmol:mol. Examination of the data revealed that between 153°E and 180° the Fe:N supply ratio is generally above 40 μmol:mol (average = 117 ± 71 μmol:mol) (Figure 11); a value that is generally regarded as the optimal Fe:N ratio for new phytoplankton production (based on an optimal Fe:C ratio of 6 μmol:mol) (Moore et al., 2004). In contrast, east of 180°, Fe:N supply ratios are more variable but generally lower than the optimum ratio of 40 μmol:mol (average = 23 ± 14 μmol:mol). Because these ratios represent the supply of iron and nitrogen into the euphotic zone, they will set the overall stoichiometry for new production. Individual organisms within the euphotic zone may have differing iron and nitrogen requirements (Sunda & Huntsman, 2015). For instance, organisms such as *Prochlorococcus* cannot readily utilize nitrate (Moore et al., 2002); thus, it will utilize other nitrogen species, such as ammonium, that are produced during the recycling of organic matter by the microbial community. Organisms also tend to partition themselves into various niches to utilize iron and nitrogen species across various light conditions (Johnson et al., 2006; Sunda & Huntsman, 2015). For example, nitrogen fixation occurs in the upper euphotic zone when nitrate and ammonium concentrations are low as higher concentrations can inhibit nitrogen fixation (Holl & Montoya, 2005). The surface water concentration of nitrate across the transect is low, thus diazotroph production is unlikely to be inhibited by nitrate supply. In contrast, *Synechococcus* tends to have a higher iron requirement compared to oceanic eukaryotic species and typically utilizes nitrate for growth (Johnson et al., 2006; Sunda & Huntsman, 2015).

Across the section, the active fluorescence measurements of F_v/F_m are close to the theoretical biophysical maximum (~0.55) for the resident phytoplankton groups (picocyanobacterial (*Synechococcus* and *Prochlorococcus*) and picoeukaryotes) sampled from the DCM. Based on the F_v/F_m results, it would appear that the supply of iron relative to nitrate into the euphotic zone is sufficient to support new production within the DCM (Suggett et al., 2009), although we are mindful that there will be niche phytoplankton populations within the DCM that can have differing iron and nitrogen requirements (Harrison et al.,

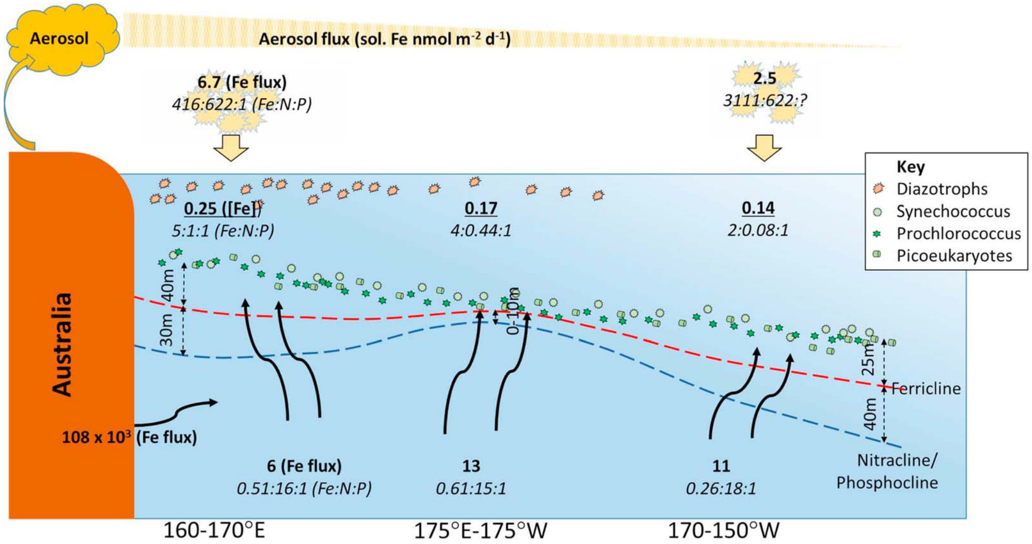

Figure 12. Conceptual figure highlighting the supply fluxes of iron, nitrogen (nitrate and ammonia), and phosphate from the atmosphere and the thermocline waters. Iron fluxes are in nmol m^{-2} d^{-1}, while Fe:N:P ratios are in units mmol:mol:mol and are based on individual supply flux. Underlined values represent dissolved iron concentration (nmol L^{-1}), and Fe:N:P ratios are in units mmol:mol:mol and are based on individual nutrient concentrations. The dominant phytoplankton groups are represented by diazotrophs, *Synechococcus*, *Prochlorococcus*, and picoeukaryotes. Also depicted are the nitracline/phosphocline and the ferricline. The atmospheric iron supply flux is based on data extracted from the Albani et al. (2014) model and converted to an iron deposition flux by assuming 3.5% w/w iron. Soluble iron was assumed to be 5%. The nitrogen deposition data at 160–170°E was calculated from data in Martino et al. (2014).

1996; Hassler et al., 2014; Johnson et al., 2006; Moore et al., 2002; Saito et al., 2014; Shiozaki et al., 2014; Sunda & Huntsman, 2015).

The lack of significant diazotroph production in surface waters between 170°W and 150°W, even though phosphate is in excess (P* = 0.099 ± 0.028 μmol L^{-1}) and iron concentrations are low (0.14 ± 0.05 nmol L^{-1}), is indicative of the SPND province found in the modeling study of Ward et al. (2013) where diazotroph production is either low or nonexistent due to iron limitation. In contrast, near continental Australia (154°E to 175°E) phosphate concentrations are generally lower (P* = 0.079 ± 0.028 μmol L^{-1}) and iron concentrations are higher (0.34 ± 0.23 nmol L^{-1}), indicative of conditions for the SPD province proposed by Ward et al. (2013) where diazotroph production occurs and hence reduce excess phosphate concentrations. This is supported by studies that have observed significantly higher rate of nitrogen fixation in the north Tasman Sea and also stimulation of nitrogen fixation by iron and dust addition in this region (Law et al., 2011).

Taking in the above information, the biogeochemistry of the Western South Pacific Ocean along the GP13 GEOTRACES section is characterized by several important characteristics, which are summarized in Figure 12 and include the following observations. There is the widespread presence of a broad DCM which deepens eastward and along the zonal section and narrows in its depth range (Figure 1). There is a large vertical gradient in the N:P ratio between the euphotic zone and the waters below with higher N:P ratios at depth (Figure 6). This indicates that the resident phytoplankton community within the DCM has a high N:P uptake ratio. Thus, the resident phytoplankton community within the DCM effectively acts like a "scrubber" whereby they almost quantitatively remove nitrate from solution such that the concentration of nitrate diffusing upward to the surface decreases to nanomolar levels. In contrast, surface phosphate concentrations are in excess relative to nitrate based on Redfield uptake stoichiometry, thereby potentially providing a niche for diazotrophs if dissolved iron concentrations are sufficient. Diazotroph production occurs close to continental Australia where iron inputs are more pronounced (Law et al., 2011, 2012; Shiozaki et al., 2014) but is low at the eastern end of the transect. This confirms previous observations of very low nitrogen fixation rates in the South Pacific Gyre (Bonnet et al., 2008). The supply of dissolved iron appears to be sufficient to support phytoplankton growth within the DCM (based on F_v/F_m values), but the dissolved iron gradient and diffusional supply flux declines eastward away from dust and continental inputs (Figure 12). Likewise, the nitracline deepens and declines away from continental landmasses.

5. Conclusions

Here we have presented high resolution iron and nutrients distributions for the GEOTRACES zonal section (GP13) extending from Australia (150°E) to the oligotrophic South Pacific Ocean gyre (150°W) between 30 and 32.5°S. Surface dissolved iron concentrations decrease eastward from generally high concentrations (>0.4 nmol L^{-1}) close to continental Australia to low concentrations (<0.2 nmol L^{-1}) within the South Pacific gyre. The higher dissolved iron concentrations are indicative of atmospheric dust and continental margin inputs near continental Australia. The zonal transport and the diffusional dissolved iron supply flux to the upper ocean (<100 m) from the thermocline also declines eastward. Using a "pipe" model from Wu and Boyle (2002), we estimate that only a small portion of the iron in remote thermocline waters (at 150°W) is sourced from the atmosphere. Across the section, the concentration of nitrate in surface waters is low and at levels that would retard phytoplankton growth. In contrast, the concentration of phosphate in surface waters is not regarded as growth limiting. Nitrogen supply into the upper ocean is primarily from deeper waters (range 24 to 1,647 μmol m^{-2} d^{-1}) with atmospheric deposition of nitrate and ammonium, and nitrogen fixation contributing less than 1% of the nitrogen supply flux. Interestingly, the deep water N:P supply flux ratio is 16 ± 3 but declines to <1 within the euphotic zone indicating that the N:P assimilation ratio for phytoplankton is >16. The stoichiometric ratio of iron and nitrogen supply into the euphotic zone averaged 47 ± 55 μmol:mol, which is close to the threshold of iron limitation for phytoplankton, although photosynthetic competence (F_v/F_m) data sets indicated that resident phytoplankton cells in the DCM are iron replete suggesting their iron requirements are being met. Placing the results from this study into the conceptual framework of Ward et al. (2013) for describing the distribution of diazotrophs and non-nitrogen-fixing marine plankton, it appears that waters near Australia fit the surplus phosphate diazotroph province with while the waters further eastward would be classified as a surplus phosphate with no diazotrophs province. The switch between these two regimes is likely connected to the supply of atmospheric iron where higher iron inputs into the euphotic zone are known to stimulate diazotroph production.

Acknowledgments
We thank the Captains and crew of the R/V *Tangaroa* and R/V *Southern Surveyor* for help at sea. We are grateful to James Moffett, Joseph Resing, and Peter Sedwick for comments on the manuscript during its development. We thank Natalie Mahowald and Sylvia Cole for providing data from their modeling efforts. We also thank Anoop Chandrasekhar for providing unpublished iron speciation data. Finally, we thank thoughtful comments from two anonymous reviewers that help to improve the manuscript. This research was supported by the New Zealand Foundation for Research, Science and Technology Coasts and Oceans Outcome-Based Investment (COIX0501), and the Australian Research Council Discovery Projects (DP1092892 and DP110100108) and Future Fellowships (FT130100037) programs, University of Tasmania, internal grants to A. R. B. (refs B0018994, B0019024, and L0018934), and University of Technology Sydney Chancellor Fellowship to CSH. The Participation of EMSW was thanks to a New Zealand International Traveller grant. The data presented in this manuscript are available from the GEOTRACE data repository (www.geotrace.org).

References

Albani, S., Mahowald, N. M., Perry, A. T., Scanza, R. A., Zender, C. S., Heavens, N. G., … Otto-Bliesner, B. L. (2014). Improved dust representation in the Community Atmosphere Model. *Journal of Advances in Modeling Earth Systems*, *6*(3), 541–570. https://doi.org/10.1002/2013MS000279

Arimoto, R., Duce, R. A., Ray, B. J., Hewitt, A. D., & Williams, J. (1987). Trace elements in the atmosphere of American Samoa: Concentrations and deposition to the tropical South Pacific. *Journal of Geophysical Research*, *92*, 8465–8479. https://doi.org/10.1029/JD092iD07p08465

Arimoto, R., Ray, B. J., Duce, R. A., Hewitt, A. D., Boldi, R., & Hudson, A. (1990). Concentrations, sources, and fluxes of trace-elements in the remote marine atmosphere of New Zealand. *Journal of Geophysical Research*, *95*, 22,389–22,405. https://doi.org/10.1029/JD095iD13p22389

Ayris, P., & Delmelle, P. (2012). Volcanic and atmospheric controls on ash iron solubility: A review. *Physics and Chemistry of the Earth, Parts A/B/C*, *45*, 103–112.

Baker, A. R., Thomas, M., Bange, H. W., & Plasencia Sánchez, E. (2016). Soluble trace metals in aerosols over the tropical south-east Pacific offshore of Peru. *Biogeosciences*, *13*(3), 817–825. https://doi.org/10.5194/bg-13-817-2016

Biller, D. V., & Bruland, K. W. (2012). Analysis of Mn, Fe, Co, Ni, Cu, Zn, Cd, and Pb in seawater using the Nobias-chelate PA1 resin and magnetic sector inductively coupled plasma mass spectrometry (ICP-MS). *Marine Chemistry*, *130-131*, 12–20. https://doi.org/10.1016/j.marchem.2011.12.001

Blain, S., Bonnet, S., & Guieu, C. (2008). Dissolved iron distribution in the tropical and sub tropical South Eastern Pacific. *Biogeosciences*, *5*, 269–280. https://doi.org/10.5194/bg-5-269-2008

Bonnet, S., Guieu, C., Bruyant, F., Prášil, O., van Wambeke, F., Raimbault, P., … Claustre, H. (2008). Nutrient limitation of primary productivity in the Southeast Pacific (BIOSOPE cruise). *Biogeosciences*, *5*, 215–225. https://doi.org/10.5194/bg-5-215-2008

Bowie, A. R., Lannuzel, D., Remenyi, T. A., Wagener, T., Lam, P. J., Boyd, P. W., … Trull, T. W. (2009). Biogeochemical iron budgets of the Southern Ocean south of Australia: Decoupling of iron and nutrient cycles in the subantarctic zone by the summertime supply. *Global Biogeochemical Cycles*, *23*, GB4034. https://doi.org/10.1029/2009GB003500

Boyd, P. W., & Ellwood, M. J. (2010). The biogeochemical cycle of iron in the ocean. *Nature Geoscience*, *3*(10), 675–682. https://doi.org/10.1038/ngeo964

Boyd, P. W., Ellwood, M. J., Tagliabue, A., & Twining, B. S. (2017). Biotic and abiotic retention, recycling and remineralization of metals in the ocean. *Nature Geoscience*, *10*(3), 167–173. https://doi.org/10.1038/ngeo2876

Boyd, P. W., & Tagliabue, A. (2015). Using the *L** concept to explore controls on the relationship between paired ligand and dissolved iron concentrations in the ocean. *Marine Chemistry*, *173*, 52–66. https://doi.org/10.1016/j.marchem.2014.12.003

Boyle, E. A., Bergquist, P. A., Kayser, R. A., & Mahowald, N. (2005). Iron, manganese, and lead at Hawaii Ocean Time-series station ALOHA: Temporal variability and an intermediate water hydrothermal plume. *Geochimica et Cosmochimica Acta*, *69*(4), 933–952. https://doi.org/10.1016/j.gca.2004.07.034

Bruland, K. W., Orians, K. J., & Cowen, J. P. (1994). Reactive trace metals in the stratified Central North Pacific. *Geochimica et Cosmochimica Acta*, *58*(15), 3171–3182. https://doi.org/10.1016/0016-7037(94)90044-2

Buck, C. S., Landing, W. M., & Resing, J. (2013). Pacific Ocean aerosols: Deposition and solubility of iron, aluminum, and other trace elements. *Marine Chemistry*, *157*, 117–130. https://doi.org/10.1016/j.marchem.2013.09.005

Chance, R., Jickells, T. D., & Baker, A. R. (2015). Atmospheric trace metal concentrations, solubility and deposition fluxes in remote marine air over the south-east Atlantic. *Marine Chemistry*, *177*(Part 1), 45–56. https://doi.org/10.1016/j.marchem.2015.06.028

Chappell, P. D., Moffett, J. W., Hynes, A. M., & Webb, E. A. (2012). Molecular evidence of iron limitation and availability in the global diazotroph *Trichodesmium*. *The ISME Journal*, *6*(9), 1728–1739.

Chiswell, S. M. (2013). Lagrangian time scales and eddy diffusivity at 1000 m compared to the surface in the South Pacific and Indian Oceans. *Journal of Physical Oceanography*, *43*(12), 2718–2732. https://doi.org/10.1175/jpo-d-13-044.1

Chiswell, S. M., Bostock, H. C., Sutton, P. J. H., & Williams, M. J. M. (2015). Physical oceanography of the deep seas around New Zealand: A review. *New Zealand Journal of Marine and Freshwater Research*, *49*(2), 286–317. https://doi.org/10.1080/00288330.2014.992918

Cole, S. T., Wortham, C., Kunze, E., & Owens, W. B. (2015). Eddy stirring and horizontal diffusivity from Argo float observations: Geographic and depth variability. *Geophysical Research Letters*, *42*, 3989–3997. https://doi.org/10.1002/2015GL063827

Croot, P. L., Streu, P., & Baker, A. R. (2004). Short residence time for iron in surface seawater impacted by atmospheric dry deposition from Saharan dust events. *Geophysical Research Letters*, *31*, L23S08. https://doi.org/10.1029/2004GL020153

Cropp, R. A., Gabric, A. J., Levasseur, M., McTainsh, G. H., Bowie, A., Hassler, C. S., … Viscarra Rossel, R. (2013). The likelihood of observing dust-stimulated phytoplankton growth in waters proximal to the Australian continent. *Journal of Marine Systems*, *117-118*, 43–52. https://doi.org/10.1016/j.jmarsys.2013.02.013

de Baar, H. J. W., Dejong, J. T. M., Bakker, D. C. E., Loscher, B. M., Veth, C., Bathmann, U., & Smetacek, V. (1995). Importance of iron for plankton blooms and carbon dioxide drawdown in the Southern Ocean. *Nature*, *373*(6513), 412–415. https://doi.org/10.1038/373412a0

de Boyer Montégut, C., Madec, G., Fischer, A. S., Lazar, A., & Iudicone, D. (2004). Mixed layer depth over the global ocean: An examination of profile data and a profile-based climatology. *Journal of Geophysical Research*, *109*, C12003. https://doi.org/10.1029/2004JC002378

Desboeufs, K., Leblond, N., Wagener, T., Bon Nguyen, E., & Guieu, C. (2014). Chemical fate and settling of mineral dust in surface seawater after atmospheric deposition observed from dust seeding experiments in large mesocosms. *Biogeosciences*, *11*(19), 5581–5594. https://doi.org/10.5194/bg-11-5581-2014

Draxler, R. R., & Hess, G. D. (1998). An overview of the HYSPLIT_4 modelling system for trajectories, dispersion and deposition. *Australian Meteorological Magazine*, *47*(4), 295–308.

Duce, R. A., Liss, P. S., Merrill, J. T., Atlas, E. L., Buat-Menard, P., Hicks, B. B., … Zhou, M. (1991). The atmospheric input of trace species to the world ocean. *Global Biogeochemical Cycles*, *5*, 193–259. https://doi.org/10.1029/91GB01778

Ellwood, M. J., Boyd, P. W., & Sutton, P. (2008). Winter-time dissolved iron and nutrient distributions in the Subantarctic Zone from 40–52S; 155–160E. *Geophysical Research Letters*, *35*, L11604. https://doi.org/10.1029/2008GL033699

Ellwood, M. J., Law, C. S., Hall, J., Woodward, E. M. S., Strzepek, R., Kuparinen, J., … Boyd, P. W. (2013). Relationships between nutrient stocks and inventories and phytoplankton physiological status along an oligotrophic meridional transect in the Tasman Sea. *Deep-Sea Research Part I*, *72*, 102–120. https://doi.org/10.1016/j.dsr.2012.11.001

Ellwood, M. J., Nodder, S. D., King, A., Hutchins, D. A., Wilhelm, S. W., & Boyd, P. W. (2014). Pelagic iron cycling during the subtropical spring bloom, east of New Zealand. *Marine Chemistry*, *160*, 18–33. https://doi.org/10.1016/j.marchem.2014.01.004

Falkowski, P. G., Barber, R. T., & Smetacek, V. (1998). Biogeochemical controls and feedbacks on ocean primary production. *Science*, *281*(5374), 200–206. https://doi.org/10.1126/science.281.5374.200

Finnigan, T. D., Luther, D. S., & Lukas, R. (2002). Observations of enhanced diapycnal mixing near the Hawaiian ridge. *Journal of Physical Oceanography*, *32*(11), 2988–3002. https://doi.org/10.1175/1520-0485(2002)

Fishwick, M. P., Sedwick, P. N., Lohan, M. C., Worsfold, P. J., Buck, K. N., Church, T. M., & Ussher, S. J. (2014). The impact of changing surface ocean conditions on the dissolution of aerosol iron. *Global Biogeochemical Cycles*, *28*, 1235–1250. https://doi.org/10.1002/2014GB004921

Fitzsimmons, J. N., Boyle, E. A., & Jenkins, W. J. (2014). Distal transport of dissolved hydrothermal iron in the deep South Pacific Ocean. *Proceedings of the National Academy of Sciences of the United States of America*, *111*(47), 16,654–16,661. https://doi.org/10.1073/pnas.1418778111

Fitzsimmons, J. N., Conway, T. M., Lee, J.-M., Kayser, R., Thyng, K. M., John, S. G., & Boyle, E. A. (2016). Dissolved iron and iron isotopes in the southeastern Pacific Ocean. *Global Biogeochemical Cycles*, *30*, 1372–1395. https://doi.org/10.1002/2015GB005357

Fitzsimmons, J. N., Hayes, C. T., Al-Subiai, S. N., Zhang, R., Morton, P. L., Weisend, R. E., … Boyle, E. A. (2015). Daily to decadal variability of size-fractionated iron and iron-binding ligands at the Hawaii Ocean Time-series Station ALOHA. *Geochimica et Cosmochimica Acta*, *171*, 303–324. https://doi.org/10.1016/j.gca.2015.08.012

Frew, R., Bowie, A., Croot, P., & Pickmere, S. (2001). Macronutrient and trace-metal geochemistry of an in situ iron-induced Southern Ocean bloom. *Deep-Sea Research Part II*, *48*(11-12), 2467–2481. https://doi.org/10.1016/S0967-0645(01)00004-2

Gabric, A. J., Cropp, R., McTainsh, G., Butler, H., Johnston, B. M., O'Loingsigh, T., & Van Tran, D. (2016). Tasman Sea biological response to dust storm events during the austral spring of 2009. *Marine and Freshwater Research*, *67*(8), 1090–1102. https://doi.org/10.1071/MF14321

GEOTRACES (2007). Report of the GEOTRACES Pacific Basin planning workshop (Rep., pp. 66). Honolulu.

Halm, H., Lam, P., Ferdelman, T. G., Lavik, G., Dittmar, T., LaRoche, J., … Kuypers, M. M. M. (2012). Heterotrophic organisms dominate nitrogen fixation in the South Pacific Gyre. *The ISME Journal*, *6*(6), 1238–1249.

Halstead, M. J. R., Cunninghame, R. G., & Hunter, K. A. (2000). Wet deposition of trace metals to a remote site in Fiordland, New Zealand. *Atmospheric Environment*, *34*(4), 665–676. https://doi.org/10.1016/S1352-2310(99)00185-5

Harrison, W. G., Harris, L. R., & Irwin, B. D. (1996). The kinetics of nitrogen utilization in the oceanic mixed layer: Nitrate and ammonium interactions at nanomolar concentrations. *Limnology and Oceanography*, *41*(1), 16–32. https://doi.org/10.4319/lo.1996.41.1.0016

Hassler, C. S., Ridgway, K. R., Bowie, A. R., Butler, E. C. V., Clementson, L. A., Doblin, M. A., … Ellwood, M. J. (2014). Primary productivity induced by iron and nitrogen in the Tasman Sea: An overview of the PINTS expedition. *Marine and Freshwater Research*, *65*(6), 517–537. https://doi.org/10.1071/MF13137

Hassler, C. S., van den Berg, C. M. G., & Boyd, P. W. (2017). Toward a regional classification to provide a more inclusive examination of the ocean biogeochemistry of iron-binding ligands. *Frontiers in Marine Science*, *4*(19). https://doi.org/10.3389/fmars.2017.00019

Hatta, M., Measures, C. I., Wu, J., Roshan, S., Fitzsimmons, J. N., Sedwick, P., & Morton, P. (2015). An overview of dissolved Fe and Mn distributions during the 2010–2011 U.S. GEOTRACES north Atlantic cruises: GEOTRACES GA03. *Deep-Sea Research Part II*, *116*, 117–129. https://doi.org/10.1016/j.dsr2.2014.07.005

Holl, C. M., & Montoya, J. P. (2005). Interactions between nitrate uptake and nitrogen fixation in continuous cultures of the marine diazotroph *Trichodesmium* (cyanobacteria). *Journal of Phycology*, *41*(6), 1178–1183. https://doi.org/10.1111/j.1529-8817.2005.00146.x

Hopkinson, B. M., & Barbeau, K. A. (2008). Interactive influences of iron and light limitation on phytoplankton at subsurface chlorophyll maxima in the eastern North Pacific. *Limnology and Oceanography*, *53*(4), 1303–1318. https://doi.org/10.4319/lo.2008.53.4.1303

Jenkins, W. J., Elder, K. L., McNichol, A. P., & von Reden, K. (2010). The passage of the bomb radiocarbon pulse into the Pacific Ocean. *Radiocarbon*, *52*(03), 1182–1190. https://doi.org/10.1017/S0033822200046257

Johnson, I. Z., Zinser, E. R., Coe, A., McNulty, N. P., Woodward, E. M. S., & Chisholm, S. W. (2006). Niche partitioning among *Prochlorococcus* ecotypes along ocean-scale environmental gradients. *Science*, *311*(5768), 1737–1740. https://doi.org/10.1126/science.1118052

Johnson, K. S., Gordon, R. M., & Coale, K. H. (1997). What controls dissolved iron concentrations in the world ocean? Authors' closing comments. *Marine Chemistry*, *57*(3-4), 181–186. https://doi.org/10.1016/S0304-4203(97)00047-9

Kretz, C. B., Bell, D. W., Lomas, D. A., Lomas, M. W., & Martiny, A. C. (2015). Influence of growth rate on the physiological response of marine *Synechococcus* to phosphate limitation. *Frontiers in Microbiology*, *6*, 85. https://doi.org/10.3389/fmicb.2015.00085

Lagerström, M. E., Field, M. P., Séguret, M., Fischer, L., Hann, S., & Sherrell, R. M. (2013). Automated on-line flow-injection ICP-MS determination of trace metals (Mn, Fe, Co, Ni, Cu and Zn) in open ocean seawater: Application to the GEOTRACES program. *Marine Chemistry*, *155*, 71–80. https://doi.org/10.1016/j.marchem.2013.06.001

Landry, M. R., Barber, R. T., Bidare, R. R., Chai, F., Coale, K. H., Dam, H. G., … White, J. R. (1997). Iron and grazing constraints on primary production in the central equatorial Pacific: An EqPac synthesis. *Limnology and Oceanography*, *42*(3), 405–418. https://doi.org/10.4319/lo.1997.42.3.0405

Law, C. S., Abraham, E. R., Watson, A. J., & Liddicoat, M. I. (2003). Vertical eddy diffusion and nutrient supply to the surface mixed layer of the Antarctic Circumpolar Current. *Journal of Geophysical Research*, *108*(C8), 3272. https://doi.org/10.1029/2002JC001604

Law, C. S., Breitbarth, E., Hoffmann, L. J., McGraw, C. M., Langlois, R. J., LaRoche, J., … Safi, K. A. (2012). No stimulation of nitrogen fixation by non-filamentous diazotrophs under elevated CO_2 in the South Pacific. *Global Change Biology*, *18*(10), 3004–3014. https://doi.org/10.1111/j.1365-2486.2012.02777.x

Law, C. S., Martin, A. P., Liddicoat, M. I., Watson, A. J., Richards, K. J., & Woodward, E. M. S. (2001). A Lagrangian SF6 tracer study of an anticyclonic eddy in the North Atlantic: Patch evolution, vertical mixing and nutrient supply to the mixed layer. *Deep-Sea Research Part II: Topical Studies in Oceanography*, *48*(4-5), 705–724. https://doi.org/10.1016/S0967-0645(00)00112-0

Law, C. S., Woodward, E. M. S., Ellwood, M. J., Marriner, A., Bury, S. J., & Safi, K. A. (2011). Response of surface nutrient inventories and nitrogen fixation to a tropical cyclone in the southwest Pacific. *Limnology and Oceanography*, *56*(4), 1372–1385. https://doi.org/10.4319/lo.2011.56.4.1372

Ledwell, J. R., Watson, A. J., & Law, C. S. (1993). Evidence for slow mixing across the pycnocline from an open-ocean tracer-release experiment. *Nature*, *364*(6439), 701–703. https://doi.org/10.1038/364701a0

Letscher, R. T., Primeau, F., & Moore, J. K. (2016). Nutrient budgets in the subtropical ocean gyres dominated by lateral transport. *Nature Geoscience*, *9*(11), 815–819. https://doi.org/10.1038/ngeo2812

Lewis, M. R., Hebert, D., Harrison, W. G., Platt, T., & Oakey, N. S. (1986). Vertical nitrate fluxes in the oligotrophic ocean. *Science*, *234*(4778), 870–873. https://doi.org/10.1126/science.234.4778.870

Li, F., Ginoux, P., & Ramaswamy, V. (2008). Distribution, transport, and deposition of mineral dust in the Southern Ocean and Antarctica: Contribution of major sources. *Journal of Geophysical Research*, *113*, D10207. https://doi.org/10.1029/2007JD009190

Mackie, D. S., Boyd, P. W., McTainsh, G. H., Tindale, N. W., Westberry, T. K., & Hunter, K. A. (2008). Biogeochemistry of iron in Australian dust: From eolian uplift to marine uptake. *Geochemistry, Geophysics, Geosystems*, *9*, Q03Q08. https://doi.org/10.1029/2007GC001813

Martin, J. H., & Fitzwater, S. E. (1988). Iron-deficiency limits phytoplankton growth in the Northeast Pacific Subarctic. *Nature*, *331*(6154), 341–343. https://doi.org/10.1038/331341a0

Martin, J. H., Knauer, G. A., Karl, D. M., & Broenkow, W. W. (1987). VERTEX: Carbon cycling in the Northeast Pacific. *Deep Sea Research Part A. Oceanographic Research Papers*, *34*(2), 267–285. https://doi.org/10.1016/0198-0149(87)90086-0

Martino, M., Hamilton, D., Baker, A. R., Jickells, T. D., Bromley, T., Nojiri, Y., … Boyd, P. W. (2014). Western Pacific atmospheric nutrient deposition fluxes, their impact on surface ocean productivity. *Global Biogeochemical Cycles*, *28*, 712–728. https://doi.org/10.1002/2013GB004794

Mawji, E., Schlitzer, R., Dodas, E. M., Abadie, C., Abouchami, W., Anderson, R. F., … Zimmer, L. A. (2015). The GEOTRACES intermediate data product 2014. *Marine Chemistry*, *177*(Part 1), 1–8. https://doi.org/10.1016/j.marchem.2015.04.005

Milne, A., Landing, W., Bizimis, M., & Morton, P. (2010). Determination of Mn, Fe, co, Ni, Cu, Zn, Cd and Pb in seawater using high resolution magnetic sector inductively coupled mass spectrometry (HR-ICP-MS). *Analytica Chimica Acta*, *665*(2), 200–207. https://doi.org/10.1016/j.aca.2010.03.027

Moisander, P. H., Zhang, R., Boyle, E. A., Hewson, I., Montoya, J. P., & Zehr, J. P. (2012). Analogous nutrient limitations in unicellular diazotrophs and *Prochlorococcus* in the South Pacific Ocean. *The ISME Journal*, *6*(4), 733–744.

Montoya, J. P., Voss, M., Kahler, P., & Capone, D. G. (1996). A simple, high-precision, high-sensitivity tracer assay for N(inf2) fixation. *Applied and Environmental Microbiology*, *62*(3), 986–993.

Moore, C. M., Mills, M. M., Arrigo, K. R., Berman-Frank, I., Bopp, L., Boyd, P. W., … Ulloa, O. (2013). Processes and patterns of oceanic nutrient limitation. *Nature Geoscience*, *6*(9), 701–710. https://doi.org/10.1038/ngeo1765

Moore, J. K., Doney, S. C., & Lindsay, K. (2004). Upper ocean ecosystem dynamics and iron cycling in a global three-dimensional model. *Global Biogeochemical Cycles*, *18*, GB4028. https://doi.org/10.1029/2004GB002220

Moore, L. R., Post, A. F., Rocap, G., & Chisholm, S. W. (2002). Utilization of different nitrogen sources by the marine cyanobacteria *Prochlorococcus* and *Synechococcus*. *Limnology and Oceanography*, *47*(4), 989–996. https://doi.org/10.4319/lo.2002.47.4.0989

Nakamae, K., Uchino, O., Morino, I., Liley, B., Sakai, T., Nagai, T., & Yokota, T. (2014). Lidar observation of the 2011 Puyehue-Cordón Caulle volcanic aerosols at Lauder, New Zealand. *Atmospheric Chemistry and Physics*, *14*(22), 12,099–12,108. https://doi.org/10.5194/acp-14-12099-2014

Okubo, A. (1971). Oceanic diffusion diagrams. *Deep Sea Research and Oceanographic Abstracts*, *18*(8), 789–802. https://doi.org/10.1016/0011-7471(71)90046-5

Osborn, T. R. (1980). Estimates of the local rate of vertical diffusion from dissipation measurements. *Journal of Physical Oceanography*, *10*(1), 83–89. https://doi.org/10.1175/1520-0485(1980)010%3C0083:eotlro%3E2.0.co;2

Palter, J. B., Marinov, I., Sarmiento, J. L., & Gruber, N. (2013). Large-scale, persistent nutrient fronts of the World Ocean: Impacts on biogeochemistry. In I. M. Belkin (Ed.), *Chemical Oceanography of Frontal Zones* (pp. 1–38). Berlin, Heidelberg: Springer. https://doi.org/10.1007/698_2013_241

Powell, C. F., Baker, A. R., Jickells, T. D., Bange, H. W., Chance, R. J., & Yodle, C. (2015). Estimation of the atmospheric flux of nutrients and trace metals to the eastern tropical North Atlantic Ocean. *Journal of the Atmospheric Sciences*, *72*(10), 4029–4045. https://doi.org/10.1175/JAS-D-15-0011.1

Queroue, F., Townsend, A. T., van der Merwe, P., Lannuzel, D., Sarthou, G., & Bowie, A. R. (2014). Advances in the offline trace metal extraction of Mn, Co, Ni, Cu, Cd, and Pb from open ocean seawater samples with determination by sector field ICP-MS analysis. *Analytical Methods*, *6*(9), 2837–2847. https://doi.org/10.1039/c3ay41312h

Raimbault, P., & Garcia, N. (2008). Evidence for efficient regenerated production and dinitrogen fixation in nitrogen-deficient waters of the South Pacific Ocean: Impact on new and export production estimates. *Biogeosciences*, *5*(2), 323–338. https://doi.org/10.5194/bg-5-323-2008

Raimbault, P., Garcia, N., & Cerutti, F. (2008). Distribution of inorganic and organic nutrients in the South Pacific Ocean—Evidence for long-term accumulation of organic matter in nitrogen-depleted waters. *Biogeosciences*, *5*(2), 281–298. https://doi.org/10.5194/bg-5-281-2008

Resing, J. A., Sedwick, P. N., German, C. R., Jenkins, W. J., Moffett, J. W., Sohst, B. M., & Tagliabue, A. (2015). Basin-scale transport of hydrothermal dissolved metals across the South Pacific Ocean. *Nature*, *523*(7559), 200–203. https://doi.org/10.1038/nature14577

Ridgway, K. R., & Dunn, J. R. (2007). Observational evidence for a Southern Hemisphere oceanic supergyre. *Geophysical Research Letters*, *34*, L13612. https://doi.org/10.1029/2007GL030392

Rijkenberg, M. J. A., Steigenberger, S., Powell, C. F., van Haren, H., Patey, M. D., Baker, A. R., & Achterberg, E. P. (2012). Fluxes and distribution of dissolved iron in the eastern (sub-)tropical North Atlantic Ocean. *Global Biogeochemical Cycles*, *26*, GB3004. https://doi.org/10.1029/2011GB004264

Rogan, N., Achterberg, E. P., Le Moigne, F. A. C., Marsay, C. M., Tagliabue, A., & Williams, R. G. (2016). Volcanic ash as an oceanic iron source and sink. *Geophysical Research Letters*, *43*, 2732–2740. https://doi.org/10.1002/2016GL067905

Saito, M. A., McIlvin, M. R., Moran, D. M., Goepfert, T. J., DiTullio, G. R., Post, A. F., & Lamborg, C. H. (2014). Multiple nutrient stresses at intersecting Pacific Ocean biomes detected by protein biomarkers. *Science*, *345*(6201), 1173–1177. https://doi.org/10.1126/science.1256450

Schlitzer, R. (2006). Ocean data view. Retrieved from http://odv.awi-bremerhaven

Sedwick, P. N., Church, T. M., Bowie, A. R., Marsay, C. M., Ussher, S. J., Achilles, K. M., … McGillicuddy, D. J. (2005). Iron in the Sargasso Sea (Bermuda Atlantic Time-series Study region) during summer: Eolian imprint, spatiotemporal variability, and ecological implications. *Global Biogeochemical Cycles*, *19*, GB4006. https://doi.org/10.1029/2004GB002445

Shaw, E. C., Gabric, A. J., & McTainsh, G. H. (2008). Impacts of aeolian dust deposition on phytoplankton dynamics in Queensland coastal waters. *Marine and Freshwater Research*, *59*(11), 951–962. https://doi.org/10.1071/MF08087

Shiozaki, T., Kodama, T., & Furuya, K. (2014). Large-scale impact of the island mass effect through nitrogen fixation in the western South Pacific Ocean. *Geophysical Research Letters*, *41*, 2907–2913. https://doi.org/10.1002/2014GL059835

Sohrin, Y., Urushihara, S., Nakatsuka, S., Kono, T., Higo, E., Minami, T., … Umetani, S. (2008). Multielemental determination of GEOTRACES key trace metals in seawater by ICPMS after preconcentration using an ethylenediaminetriacetic acid chelating resin. *Analytical Chemistry*, *80*(16), 6267–6273. https://doi.org/10.1021/ac800500f

Stein, A. F., Draxler, R. R., Rolph, G. D., Stunder, B. J. B., Cohen, M. D., & Ngan, F. (2015). NOAA's HYSPLIT atmospheric transport and dispersion modeling system. *Bulletin of the American Meteorological Society*, *96*(12), 2059–2077. https://doi.org/10.1175/BAMS-D-14-00110.1

Stevens, C. L., Consalvey, M., Devine, J. A., & Clark, M. R. (2014). Mixing and transport near the shallow-crested Rumble III seamount and the implications for plankton distribution. *New Zealand Journal of Marine and Freshwater Research*, *48*(2), 194–215. https://doi.org/10.1080/00288330.2013.872154

Stevens, C. L., Sutton, P. J., & Law, C. S. (2012). Internal waves downstream of the Norfolk Ridge, western Pacific, and their biophysical implications. *Limnology and Oceanography*, *57*(4), 897–911. https://doi.org/10.4319/lo.2012.57.4.0897

Suggett, D. J., Moore, C. M., Hickman, A., & Geider, R. J. (2009). Interpretation of fast repetition rate (FRR) fluorescence: Signatures of phytoplankton community structure versus physiological state. *Marine Ecology Progress Series*, *376*, 1–19. https://doi.org/10.3354/meps07830

Sunda, W. G., & Huntsman, S. A. (2015). High iron requirement for growth, photosynthesis, and low-light acclimation in the coastal cyanobacterium *Synechococcus bacillaris*. *Frontiers in Microbiology*, *6*, 561. https://doi.org/10.3389/fmicb.2015.00561

Tagliabue, A., Sallee, J.-B., Bowie, A. R., Levy, M., Swart, S., & Boyd, P. W. (2014). Surface-water iron supplies in the Southern Ocean sustained by deep winter mixing. *Nature Geoscience*, *7*(4), 314–320. https://doi.org/10.1038/ngeo2101

Twining, B. S., Nodder, S. D., King, A. L., Hutchins, D. A., LeCleir, G. R., DeBruyn, J. M., … Boyd, P. W. (2014). Differential remineralization of major and trace elements in sinking diatoms. *Limnology and Oceanography*, *59*(3), 689–704. https://doi.org/10.4319/lo.2014.59.3.0689

Van Wambeke, F., Bonnet, S., Moutin, T., Raimbault, P., Alarcón, G., & Guieu, C. (2008). Factors limiting heterotrophic bacterial production in the southern Pacific Ocean. *Biogeosciences*, *5*(3), 833–845. https://doi.org/10.5194/bg-5-833-2008

Völker, C., & Tagliabue, A. (2015). Modeling organic iron-binding ligands in a three-dimensional biogeochemical ocean model. *Marine Chemistry*, *173*, 67–77. https://doi.org/10.1016/j.marchem.2014.11.008

Wagener, T., Guieu, C., Losno, R., Bonnet, S., & Mahowald, N. (2008). Revisiting atmospheric dust export to the Southern Hemisphere ocean: Biogeochemical implications. *Global Biogeochemical Cycles*, *22*, GB2006. https://doi.org/10.1029/2007GB002984

Ward, B. A., Dutkiewicz, S., Moore, C. M., & Follows, M. J. (2013). Iron, phosphorus, and nitrogen supply ratios define the biogeography of nitrogen fixation. *Limnology and Oceanography*, *58*(6), 2059–2075. https://doi.org/10.4319/lo.2013.58.6.2059

Wessel, P., & Smith, W. H. F. (1998). New, improved version of generic mapping tools released. *Eos, Transactions American Geophysical Union*, *79*(47), 579–579. https://doi.org/10.1029/98EO00426

Wijffels, S. E., Toole, J. M., & Davis, R. (2001). Revisiting the South Pacific subtropical circulation: A synthesis of World Ocean Circulation Experiment observations along 32°S. *Journal of Geophysical Research*, *106*, 19,481–19,513. https://doi.org/10.1029/1999JC000118

Woodward, E. M. S. (2002). Nanomolar detection for phosphate and nitrate using liquid waveguide technology. *Eos, Transactions American Geophysical Union*, *83*, 92.

Woodward, E. M. S., & Rees, A. P. (2001). Nutrient distributions in an anticyclonic eddy in the northeast Atlantic Ocean, with reference to nanomolar ammonium concentrations. *Deep-Sea Research Part II*, *48*(4-5), 775–793. https://doi.org/10.1016/S0967-0645(00)00097-7

Wu, J. F., & Boyle, E. A. (2002). Iron in the Sargasso Sea: Implications for the processes controlling dissolved Fe distribution in the ocean. *Global Biogeochemical Cycles*, *16*(4), 1086. https://doi.org/10.1029/2001GB001453

Zhurbas, V., & Oh, I. S. (2004). Drifter-derived maps of lateral diffusivity in the Pacific and Atlantic oceans in relation to surface circulation patterns. *Journal of Geophysical Research*, *109*, C05015. https://doi.org/10.1029/2003JC002241